A KDE-based random walk method for modeling reactive transport with complex kinetics in porous media

Guillem Sole-Mari[1,2], Daniel Fernàndez-Garcia[1,2], Paula Rodríguez-Escales[1,2], Xavier Sanchez-Vila[1,2]

[1]Department of Civil and Environmental Engineering (DECA), Universitat Politècnica de Catalunya (UPC), Jordi Girona 1-3, 08034 Barcelona, Spain.

[2]Associated Unit: Hydrogeology Group (UPC-CSIC).

Corresponding author: Guillem Sole-Mari (guillem.sole.mari@upc.edu)

Key points

- A Random Walk Particle Tracking Method capable to simulate reactions with complex kinetics is presented
- Particles are equipped with optimal kernels to represent the uncertainty in the particle position driven by subsampling a large population
- The method is implemented in a column transport model and tested for four different reactive transport case examples

Abstract

In recent years a large body of literature has been devoted to study reactive transport of solutes in porous media based on pure Lagrangian formulations. Such approaches have also been extended to accommodate second-order bimolecular reactions, in which the reaction rate is proportional to the concentrations of the reactants. Rather, in some cases, chemical reactions involving two reactants follow more complicated rate laws. Some examples are (1) reaction rate laws written in terms of powers of concentrations, (2) redox reactions incorporating a limiting term (e.g. Michaelis-Menten), or (3) any reaction where the activity coefficients vary with the concentration of the reactants, just to name a few. We provide a methodology to account for complex kinetic bimolecular reactions in a fully Lagrangian framework where each particle represents a fraction of the total mass of a specific solute. The method, built as an extension to the second-order case, is based on the concept of optimal Kernel Density Estimator, which allows the concentrations to be written in terms of particle locations, hence transferring the concept of reaction rate to that of particle location distribution. By doing so, we can update the probability of particles reacting without the need to fully reconstruct the concentration maps. The performance and convergence of the method is tested for several illustrative examples that simulate the Advection-Dispersion-Reaction Equation in a 1D homogeneous column. Finally, a 2D example of application is presented evaluating the need of fully describing non-linear chemical kinetics in a randomly heterogeneous porous medium.

SCIPEDIA
Register for free at https://www.scipedia.com to download the version without the watermark

Index terms: Groundwater Transport (1832), Computational Hydrology (1805), Stochastic Hydrology (1869), Modeling (1847), Geochemical Modeling (1009)

Keywords: Reactive transport, complex kinetics, porous media, random walk, particle tracking, Kernel Density Estimators

SCIPEDIA

Register for free at https//www.scipedia.com to download the version without the watermark

1. Introduction

Random Walk Particle Tracking Methods (RWPTMs) offer a convenient Lagrangian numerical approach to simulate solute transport in porous media. RWPTMs have been demonstrated to be particularly efficient in dealing with aquifer heterogeneities and non-reactive transport involving a large variety of complex processes such as non-Fickian transport and multiple porosity systems [*Wen and Gómez-Hernández*, 1996; *LaBolle et al.*, 1996; *Sanchez-Vila and Solis-Delfin*, 1999; *Salamon et al.*, 2006a, 2006b; *Riva et al.*, 2008; *Delay and Bodin*, 2001; *Cvetkovic and Haggerty*, 2002; *Berkowitz et al.*, 2006; *Zhang and Benson*, 2008; *Dentz and Castro*, 2009; *Benson and Meerschaert*, 2009; *Tsang and Tsang*, 2001; *Huang et al.*, 2003; *Willmann et al.*, 2013; *Henri and Fernàndez-Garcia*, 2014, 2015]. This family of methods essentially consist of discretizing the solute mass (existing initially or injected through the boundaries with time) into a finite number of particles, each representing a fraction of the total mass, and then moving such particles according to simple relationships that represent the transport mechanisms considered (e.g., advection, dispersion or diffusion into stagnant zones). RWPTMs are mass conservative by construction, and avoid some of the inherent numerical difficulties associated with Eulerian approaches, i.e., numerical dispersion and oscillations [*Salamon et al.*, 2006a; *Benson et al.*, 2017].

SCIPEDIA
Register for free at https://www.scipedia.com to download the version without the watermark

However, several disadvantages have prevented the general use of RWPTMs in reactive transport problems with few limited exceptions. The main roadblock is that most chemical reactions are written in terms of concentrations (or chemical activities), which are not directly accessible at any given time, unless previously reconstructed from discrete particle information. At this stage, one needs to keep in mind that a naive reconstruction, such as the use of histograms, is an error prone process that can lead to

spurious fluctuations [e.g., *Boso et al.*, 2013]. Consequently, as concentrations - and in some cases their gradients [e.g., *De Simoni et al.*, 2007] - are reaction drivers, errors can propagate to reaction rates. Albeit recent works [*Fernàndez-Garcia and Sanchez-Vila*, 2011; *Pedretti and Fernàndez-Garcia*, 2013; *Schmidt et al.*, 2017] have shown that the spurious fluctuations of the concentrations reconstructed from particles can be largely minimized by using a post-processing analysis based on kernels, modeling complex reactive transport problems with RWPTMs is still a challenge.

The focus of this paper is on kinetic chemical reactions. In this context, several methods have been proposed in the literature to simulate reactive transport with RWPTMs. Simple linear kinetic reactive transport problems such as first-order network reactions and slow sorption can easily be treated with transition probabilities, without having to estimate the concentrations during the course of the simulations [e.g., *Kinzelbach*, 1987; *Andricevic and Foufoula-Georgiou*, 1991; *Michalak and Kitanidis*, 2000; *Henri and Fernàndez-Garcia*, 2014; 2015]. Reconstruction kernels as an efficient post-processing tool with little drawbacks.

SCIPEDIA
Register for free at https://www.scipedia.com to download the version without the watermark

However, the incorporation of non-linear chemical reactions involving more than one chemical species into the RWPTM is remarkably cumbersome. In this case, one needs to either re-estimate solute concentrations at any given time step or to use particle proximity relationships. Both these approaches present important disadvantages, which have hindered the widespread use of RWPTMs – since the most common processes in geochemistry and biogeochemistry are complex, being non-linear, multi-species and affected by water-rock interaction. The first approach is a hybrid Lagrangian-Eulerian method by which reaction rates are determined from concentrations. Here, a

compromise between CPU time and the back and forth transformation of particles to concentrations is necessary [*Tompson*, 1993; *Tompson et al*., 1996; *Cui et al*., 2014]; as aforementioned, this process is either error-prone or computationally expensive. The second approach is purely Lagrangian, and sophisticated search algorithms are needed to calculate proximity relationships [*Paster et al*., 2014]. Along this line, *Benson and Meerschaert* [2008] studied a simple bimolecular system ($A + B \rightarrow C$) with second-order kinetics, and found that the probability of reaction of two isolated particles depends on both thermodynamics and the probability of collocation of two particles. *Paster et al.* [2013, 2014] extended these concepts to higher dimensions, and *Ding and Benson* [2015] used this bimolecular type of reaction as a building block to simulate the Michaelis-Menten enzyme kinetic model. *Rahbaralam et al.* [2015] demonstrated that the support volume of particles in the probability of collocation can be determined by using an optimal kernel bandwidth approach. This method speeds up the algorithm and avoids incomplete mixing due to the use of a limited number of particles. A first field application of the *Benson and Meerschaert* [2008] method has been recently presented by *Ding et al.* [2017], who simulated the degradation of Carbon Tetrachloride at the Schoolcraft, MI site, under anaerobic conditions. All existing variations of this method share an important limitation: they can only reproduce second-order kinetics, with the exception of those complex reactions that can be modeled as a combination of first-order monomolecular reactions and second-order bimolecular reactions, such as the aforementioned Michaelis-Menten enzyme kinetic model.

SCIPEDIA
Register for free at https//www.scipedia.com to download the version without the watermark

In some other Lagrangian approaches such as SPH [e.g. *Tartakowsky and Meakin.* 2005; *Tartakovsky et al*., 2007; *Herrera et al.,* 2009, 2017] each particle represents a volume of fluid, so concentrations are directly attributed to particles and

diffusion/dispersion is simulated by exchanging mass between particles. A similar approach was used by *Benson and Bolster* [2016] to propose a particle tracking method for the simulation of chemical reactions of arbitrary complexity, based on mass exchange between particles which could contain any variety of chemical compounds. *Engdahl et al.* [2017] recently generalized the capabilities of the method by coupling it to the reaction engine PhreeqcRM [*Parkhurst and Wissmeier*, 2015]. Each particle can be seen as a mobile bin containing a fixed volume of water, and reactions occur inside particles according to the particle-specific solute concentrations. Some limitations can be attributed to these kind of methods. For instance, one needs to artificially inject empty particles in places where solutes can potentially diffuse, or to add immobile particles and use very small time steps to represent linear sorption.

Most of these approaches to Lagrangian modeling of reactive transport use kernel functions to account for either dispersion or reaction between particles. Kernels have also been widely used in other fields of science like fluid mechanics [e.g., *Wu and Li*, 2007; *Yue et al.*, 2004], computer vision and image processing [e.g., *Chang and Ansari*, 2005; *Stoessel and Sagerer*, 2006; *Takeda et al.*, 2007], or 3D animation [e.g., *Ihmsen et al.*, 2011], just to name a few.

In this paper, we propose a new random walk particle tracking method capable of simulating different sorts of complex kinetic reactions occurring between two reactants (thus generalizing the existing methods to simulate second-order kinetics), while maintaining the classical interpretation of a particle (a fraction of the total mass of a given species). To simulate reactions, we determine the probability that any particle reacts based on particle interactions, the reaction rate law and the stoichiometry. The

SCIPEDIA
Register for free at https://www.scipedia.com to download the version without the watermark

idea behind the proposed method is to equipped each particle with an optimal kernel function that defines the particle support [*Fernàndez-Garcia and Sanchez-Vila*, 2011; *Rahbaralam et al.*, 2015] from the beginning of the simulation. For convenience, complex reaction rates are expressed as the product of a second-order bimolecular reaction and a compensation function (g) that depends on the reactant concentrations. An approximate solution of the probability of reaction is then determined, providing a fully Lagrangian approach that does not entail any kind of spatial discretization. The probability of reaction is demonstrated to depend on the particle interaction, expressed as the volume integral of the product between particle kernel functions, and on the point-value of g at a weighted mid-position between the two particles.

We then show four example column transport (1D) applications to illustrate the performance and the convergence of the method as a function of the initial number of particles for different chemical systems. To achieve this, the random walk particle tracking solution is compared with a highly discretized finite difference solution that is assumed to represent the exact solution. The four examples represent a wide sample of the most common problems in biogeochemistry: two examples of non-linear aqueous reactions and two examples of non-linear reactions considering the water-rock interaction. Finally, a 2D example of application is presented evaluating the need of fully describing non-linear chemical kinetics in a randomly heterogeneous porous medium.

SCIPEDIA
Register for free at https://www.scipedia.com to download the version without the watermark

Although the example applications are 1D or 2D reactive transport problems in stationary flow, the proposed method has no limitations regarding the number of spatial dimensions or the effect of variable velocity with time (full 4D).

2. Second-order kinetic reactions

In order to lay the groundwork for the implementation of arbitrarily complex kinetic reactions, we start by reviewing some concepts and then reformulating the mathematical expressions corresponding to second-order bimolecular reactions. Let us consider a simple bimolecular irreversible reaction $\alpha\mathrm{A} + \beta\mathrm{B} \rightarrow \gamma\mathrm{C}$ with a reaction rate proportional to the concentration of both reactants,

$$r(\mathbf{x},t) = k_f\, c_{\mathrm{A}}(\mathbf{x},t)\, c_{\mathrm{B}}(\mathbf{x},t), \#(1)$$

where c_s is the concentration of the sth-species $\{s = \mathrm{A},\mathrm{B},\mathrm{C}\}$, k_f is the forward reaction coefficient, $\{\alpha,\beta,\gamma\}$ are the stoichiometric coefficients, and $r(\mathbf{x},t)$ is the reaction rate at the $\mathbf{x}$ location and time t, defined as:

SCIPEDIA
Register for free at https://www.scipedia.com to download the version without the watermark

$$r(\mathbf{x},t) = \frac{1}{\gamma}\frac{dc_{\mathrm{C}}}{dt} = -\frac{1}{\alpha}\frac{dc_{\mathrm{A}}}{dt} = -\frac{1}{\beta}\frac{dc_{\mathrm{B}}}{dt} \#(2)$$

We refer to chemical reactions that follow equation (1) as second-order kinetic reactions, also implying that the reaction is of first-order with respect to each reactant.

Although here we study an irreversible reaction, reversibility can be modeled as a combination of a forward reaction and a backward reaction. Further details are given at the end of section 3.

2.1. The particle pair annihilation method

Benson and Meerschaert [2008] found that this problem could be solved by simply analyzing how two isolated A and B particles react to form a C particle when $\alpha = \beta = 1$. Although the original expression was developed for a general application, here we present it incorporating explicitly the effect of porosity for the particular case of porous media. In one dimension, the probability of reaction of these two particles in a given time interval Δt is given by the expression,

$$P(\mathrm{A} \rightarrow \mathrm{C}, \Delta t) = \phi^{-1}\, k_f \Delta t\, m\, \frac{1}{\sqrt{4\pi h^2}} \exp\left(-\frac{(X_\mathrm{A} - X_\mathrm{B})^2}{4h^2}\right), \#(3)$$

which is obtained as the product of the probability that the two particles will occupy the same differential volume times the conditional probability that, upon collocation, the particles will react during the time step Δt. Equation (3) is written in terms of the particle mass m (or amount of substance, depending on how k_f is defined; thus, in this work the term *particle mass* is used in a general sense). Here, the mass of all particles is assumed equal to $m = \frac{\Omega\, \phi [\mathrm{A}]_0}{N_0}$, where Ω is the initial volume occupied by the injected particles, ϕ is porosity, $[\mathrm{A}]_0$ is the initial concentration of species A, and N_0 the number of A particles injected. Finally, $h = \sqrt{2D\Delta t}$ is the length of influence of one particle defined only in terms of local diffusion and/or dispersion.

SCIPEDIA
Register for free at https//www.scipedia.com to download the version without the watermark

Once the probability of reaction of two particles is calculated, chemical reactions in the random walk method can be incorporated by particle annihilation, i.e., when two particles react, they disappear. This means that the number of particles of the reactant species decreases as the simulation progresses, and numerical resolution problems may arise at low concentrations. This limitation was addressed by *Bolster et al*. [2016], who

showed that a change in the particle mass is also a valid alternative to particle annihilation.

There is another strong limitation in the particle pair annihilation method. Chemical reactions depend on the activities of the reactants rather than on their concentrations. Thus, the aforementioned approach cannot reproduce second-order reactions correctly unless the ionic strength is not affected by the reaction or its effect on the activity coefficients is negligible. This is particularly relevant when modelling reactions that have an important impact on the ionic strength of the solution.

2.2. The optimal kernel approach

2.2.1 Representation of a particle

The RWPTM satisfies the transport equation in the limit when the number of particles approaches infinity. Considering that each *i*th particle associated with species *s* at time *t* is located at a point $\mathbf{X}_s^i$, and that no size is attributed to it, its spatial distribution can be expressed as a Dirac delta distribution and then the concentration of a given species can be written formally as,

$$c_s(\mathbf{x},t) = \frac{1}{\phi(\mathbf{x})}\sum_{i=1}^{n_s} m_s^i \, E\left\{\delta\left(\mathbf{x}-\mathbf{X}_s^i(t)\right)\right\}, \#(4)$$

where m_s^i is the mass of the *i*th particle of species *s*, $\phi(\mathbf{x})$ is the location dependent porosity, and $E\{\cdot\}$ is the expectation operator over all particle realizations. The expectation of the Dirac delta function is the probability density function (pdf) of the particle position, $p_s^i(\mathbf{x};t)$. In practice, simulations cannot use an infinite number of

234 particles and the inference of $p_s^i(\mathbf{x};t)$ becomes the Achilles heel of all random walk
235 methods. Typically, the concentration field is estimated by averaging the mass over a
236 fixed support volume $V(\mathbf{x})$ centered at the $\mathbf{x}$ location. This can be achieved by counting
237 the mass of particles in fixed bins or by projection functions [*Tompson and Gelhar*,
238 1990; *Tompson et al.*, 1996]. However, these methods suffer from the same problems as
239 those associated with the estimation of pdfs through histograms, i.e., results depend on
240 the discretization of the domain or the bin size.

241

242 An alternative approach was introduced by *Fernàndez-Garcia and Sanchez-Vila* [2011].
243 The method recognizes the uncertainty associated with subsampling an infinite number
244 of particles by equipping each particle with a pdf (the kernel function). The estimation
245 of concentrations can then be written as a direct extension of (4),

$$c_s(\mathbf{x},t) = \frac{1}{\phi(\mathbf{x})}\sum_{i=1}^{n_s} m_s^i\, W\left(\mathbf{x}-\mathbf{X}_s^i\,;\mathbf{H}_s\right), \#(5)$$

246 where $\mathbf{H_s}$ is the kernel bandwidth matrix associated to species s and $W(\mathbf{u}\,;\mathbf{H})$ is the
247 scaled kernel function, for which several shapes have been suggested, the most common
248 one being the Gaussian kernel function,

$$W(\mathbf{u};\mathbf{H}) = (2\pi)^{-\frac{d}{2}}|\mathbf{H}|^{-\frac{1}{2}}\exp\left(-\frac{1}{2}\,\mathbf{u}^T\mathbf{H}^{-1}\mathbf{u}\right), \#(6)$$

249 where d is the space dimension. In the Gaussian kernel (6), the bandwidth matrix is the
250 covariance matrix. Expression (5) is valid for an infinite domain or away from the
251 domain boundaries. The particular treatment of boundaries is discussed in the
252 subsequent sections. Note that the concentration of a given species at any given $\mathbf{x}$
253 location does not depend only on the subset of particles falling into an arbitrary bin, but

254 on all existing particles associated with that species. Assuming that $\mathbf{H}_s = h_s^2\,\mathbf{I}_d$ (we will
255 refer to this case later as the isotropic kernel) the optimal bandwidth h_s associated with
256 a given species *s* (also denoted as particle support) can be determined based on the
257 amount of particles n_s and their distribution in space, by minimizing the Asymptotical
258 Mean Integrated Squared Error ($A\text{-}MISE$). This is a well-known procedure in statistics
259 [e.g., *Silverman*, 1986; *Härdle*, 1991]. For a second-order kernel,

$$h_s = \left(\frac{d\,R(W)}{R(\nabla^2 p_s)\mu_2^2(W)n_s}\right)^{\frac{1}{d+4}}, \#(7)$$

260 where R is the L_2 norm of a function, μ_2 is the second moment, and p_s is the normalized
261 concentration,

$$p_s(\mathbf{x},t) = \frac{c_s(\mathbf{x},t)}{\int_{\Omega^d} c_s(\mathbf{x},t)\,d\mathbf{x}}, \#(8)$$

262 where Ω^d is the d-dimensional domain of the model. Note that, in this setup, the
263 estimation of c_s is not explicit, i.e. the estimator (7) depends circularly on the estimation
264 (5). Hence, one needs to either use an iterative method or make an assumption on the
265 approximate shape of the particle plume. The former approach can be computationally
266 intensive, whereas the latter can lead to a suboptimal bandwidth choice, hindering the
267 convergence rate of the estimation with respect to the number of particles. We refer to
268 *Engel et al*. [1994] for details on the calculation of h_s. Since p_s in RWPTMs changes
269 over time, the kernel bandwidth matrix $\mathbf{H}_s$ is a time-dependent variable that not only
270 accounts for local diffusion and/or dispersion but also for the spreading and stretching
271 of each particle plume. This approach has been used in subsurface hydrology to
272 reconstruct key variables associated with a wide variety of problems, e.g., reaction rates
273 and mixing measures [*Fernàndez-Garcia and Sanchez-Vila*, 2011], power-law tailing in

274 breakthrough curves [*Pedretti and Fernàndez-Garcia*, 2013], and human health risk
275 estimates [*Siirila-Woodburn et al*., 2015].

276

277 **2.2.2. The probability of reaction of a particle**

278 This section derives the probability of reaction of a given particle for a second order
279 reaction with arbitrary stoichiometric coefficients. For the derivation, we assume that
280 the problem domain Ω^d is infinite, so expression (5) is valid at any location. At the end
281 of section 3 it is discussed how the methodology can be adapted to simulate reactions
282 near the boundaries of a finite domain. The chemical reaction is still represented by
283 $\alpha\mathrm{A} + \beta\mathrm{B} \rightarrow \gamma\mathrm{C}$ and the reaction rate follows equation (1). The probability that a particle
284 reacts in the time interval $[t, t + \Delta t]$ can be simply expressed as mass consumed per
285 unit of mass,

$$P\left(\mathrm{A}^i \rightarrow \mathrm{C}^k, \Delta t\right) = -\frac{\Delta m_{\mathrm{A}}^i}{m_{\mathrm{A}}^i}, \#(9)$$

$$P\left(\mathrm{B}^j \rightarrow \mathrm{C}^k, \Delta t\right) = -\frac{\Delta m_{\mathrm{B}}^j}{m_{\mathrm{B}}^j}. \#(10)$$

286 Here, A^i refers to the *i*th-particle associated with species A, $P\left(\mathrm{A}^i \rightarrow \mathrm{C}^k, \Delta t\right)$ is the
287 probability that A^i is transformed into a new particle C^k in the time interval Δt, and
288 Δm_{A}^i is the increment of mass of the particle A^i due to the chemical reaction. This
289 relationship was used by *Salamon et al*. [2007] and *Henri and Fernàndez-Garcia* [2014,
290 2015] to develop particle transition probabilities for modeling solute transport with
291 multi-rate mass transfer and network reactions. From the definition of reaction rate
292 given in (2), expressions (9) and (10) can be rewritten as:

$$P\left(\mathrm{A}^i \to \mathrm{C}^k, \Delta t\right) = \frac{\alpha}{m_{\mathrm{A}}^i} \int_t^{t+\Delta t} \int_{\Omega^d} \phi\, r_{\mathrm{A}}^i(\mathbf{x}, t')\; d\mathbf{x}\, dt' \approx \frac{\alpha}{m_{\mathrm{A}}^i}\, \Delta t \int_{\Omega^d} \phi\, r_{\mathrm{A}}^i(\mathbf{x}, t)\; d\mathbf{x}\,, \#(11)$$

$$P\left(\mathrm{B}^j \to \mathrm{C}^k, \Delta t\right) = \frac{\beta}{m_{\mathrm{B}}^j} \int_t^{t+\Delta t} \int_{\Omega^d} \phi\, r_{\mathrm{B}}^j(\mathbf{x}, t')\; d\mathbf{x}\, dt' \approx \frac{\beta}{m_{\mathrm{B}}^j}\, \Delta t \int_{\Omega^d} \phi\, r_{\mathrm{B}}^j(\mathbf{x}, t)\; d\mathbf{x}\,, \#(1$$

where $r_{\mathrm{A}}^i(\mathbf{x}, t)$ and $r_{\mathrm{B}}^j(\mathbf{x}, t)$ are particle reaction rates. The products $\alpha\, r_{\mathrm{A}}^i(\mathbf{x}, t)$ and $\beta\, r_{\mathrm{B}}^j(\mathbf{x}, t)$ define the amount of particle mass consumed per unit volume of liquid in a unit of time. The particle reaction rates can be derived as it follows. Substituting (5) into (1), it is possible to find an expression of the total chemical reaction rate as a function of particle kernel distributions,

$$r(\mathbf{x}, t) = \frac{k_f}{\phi^2} \sum_{i=1}^{n_{\mathrm{A}}} \sum_{j=1}^{n_{\mathrm{B}}} m_{\mathrm{A}}^i m_{\mathrm{B}}^j\; W\left(\mathbf{x} - \mathbf{X}_{\mathrm{A}}^i; \mathbf{H}_{\mathrm{A}}\right) W\left(\mathbf{x} - \mathbf{X}_{\mathrm{B}}^j; \mathbf{H}_{\mathrm{B}}\right). \#(13)$$

The reaction rate of any particle A^i or B^j is determined, respectively, from the interaction of A^i with all existing B-particles and the interaction of B^j with all existing A-particles. Thus, the total reaction rate can be decomposed as

$$r(\mathbf{x}, t) = \sum_{i=1}^{n_{\mathrm{A}}} r_{\mathrm{A}}^i(\mathbf{x}, t) = \sum_{j=1}^{n_{\mathrm{B}}} r_{\mathrm{B}}^j(\mathbf{x}, t)\,, \#(14)$$

where

$$r_{\mathrm{A}}^i(\mathbf{x}, t) = \frac{k_f}{\phi^2} m_{\mathrm{A}}^i \sum_{j=1}^{n_{\mathrm{B}}} m_{\mathrm{B}}^j\; W\left(\mathbf{x} - \mathbf{X}_{\mathrm{A}}^i; \mathbf{H}_{\mathrm{A}}\right) W\left(\mathbf{x} - \mathbf{X}_{\mathrm{B}}^j; \mathbf{H}_{\mathrm{B}}\right), \#(15)$$

$$r_{\mathrm{B}}^j(\mathbf{x}, t) = \frac{k_f}{\phi^2} m_{\mathrm{B}}^j \sum_{i=1}^{n_A} m_{\mathrm{A}}^i\; W\left(\mathbf{x} - \mathbf{X}_{\mathrm{A}}^i; \mathbf{H}_{\mathrm{A}}\right) W\left(\mathbf{x} - \mathbf{X}_{\mathrm{B}}^j; \mathbf{H}_{\mathrm{B}}\right). \#(16)$$

Each term in the summation represents the interaction between two individual particles A^i and B^j. In the particular case of a Gaussian kernel function, the kernel product can be rewritten as

$$W\left(\mathbf{x}-\mathbf{X}_{\mathrm{A}}^{i};\mathbf{H}_{\mathrm{A}}\right)W\left(\mathbf{x}-\mathbf{X}_{\mathrm{B}}^{j};\mathbf{H}_{\mathrm{B}}\right)=W\left(\mathbf{x}-\mathbf{X}_{\mathrm{AB}}^{ij};\mathbf{H}_{\mathrm{AB}}\right)W\left(\mathbf{X}_{\mathrm{A}}^{i}-\mathbf{X}_{\mathrm{B}}^{j};\mathbf{H}_{\mathrm{A}}+\mathbf{H}_{\mathrm{B}}\right),\#(17)$$

where

$$\mathbf{H}_{\mathrm{AB}}=(\mathbf{H}_{\mathrm{A}}^{-1}+\mathbf{H}_{\mathrm{B}}^{-1})^{-1},\#(18)$$

$$\mathbf{X}_{\mathrm{AB}}^{ij}=\mathbf{H}_{\mathrm{AB}}\left(\mathbf{H}_{\mathrm{A}}^{-1}\mathbf{X}_{\mathrm{A}}^{i}+\mathbf{H}_{\mathrm{B}}^{-1}\mathbf{X}_{\mathrm{B}}^{j}\right),\#(19)$$

which means that the product of two Gaussian kernel density functions associated with particles A^i and B^j is proportional to another Gaussian kernel function centered at $\mathbf{X}_{\mathrm{AB}}^{ij}$ with a covariance matrix $\mathbf{H}_{\mathrm{AB}}$. Figure 1 illustrates this equivalence in one dimension. This indicates that the reaction between two individual particles is occurring mostly around $\mathbf{X}_{\mathrm{AB}}^{ij}$. The second kernel function on the right hand side of (17) is a constant scaling factor that only depends on the separation between particles.

In the case where $\mathbf{H}_{\mathrm{A}}$ and $\mathbf{H}_{\mathrm{B}}$ are isotropic ($\mathbf{H}_s=h_s^2\mathbf{I}_d$), then it derives from (18) that $\mathbf{H}_{\mathrm{AB}}$ is also isotropic ($\mathbf{H}_{\mathrm{AB}}=h_{\mathrm{AB}}^2\mathbf{I}_d$) and

$$h_{\mathrm{AB}}=\sqrt{\frac{h_{\mathrm{A}}^2h_{\mathrm{B}}^2}{h_{\mathrm{A}}^2+h_{\mathrm{B}}^2}}\#(20)$$

is proportional to the harmonic mean of the squares of $h_{\mathrm{A}},h_{\mathrm{B}}$. As aforementioned, $\mathbf{X}_{\mathrm{AB}}^{ij}$ is the position with maximum probability density of collocation of particles A^i and B^j; in the isotropic case, expression (19) can be rewritten so that $\mathbf{X}_{\mathrm{AB}}^{ij}$ is simply the mid-

position of the particle pair weighted by their corresponding squared particle support, i.e.,

$$\mathbf{X}_{\mathrm{AB}}^{ij} = \frac{\mathbf{X}_{\mathrm{A}}^{i}\, h_{\mathrm{B}}^{2} + \mathbf{X}_{\mathrm{B}}^{j} h_{\mathrm{A}}^{2}}{h_{\mathrm{A}}^{2} + h_{\mathrm{B}}^{2}}. \#(21)$$

In order to integrate expressions (11) and (12), we assume a locally constant porosity over the kernel product support centered at $\mathbf{X}_{\mathrm{AB}}^{ij}$ and represented by $\mathbf{H}_{\mathrm{AB}}$. By substituting (15) and (16) into (11) and (12) respectively and integrating, we finally obtain that

$$P\left(\mathrm{A}^{i} \rightarrow \mathrm{C}^{k}, \Delta t\right) = \frac{\alpha\, k_f}{\phi(\mathbf{X}_{\mathrm{AB}}^{ij})} \Delta t \sum_{j=1}^{n_{\mathrm{B}}} m_{\mathrm{B}}^{j}\, W\left(\mathbf{X}_{\mathrm{A}}^{i} - \mathbf{X}_{\mathrm{B}}^{j}; \mathbf{H}_{\mathrm{A}} + \mathbf{H}_{\mathrm{B}}\right), \#(22)$$

$$P\left(\mathrm{B}^{j} \rightarrow \mathrm{C}^{k}, \Delta t\right) = \frac{\beta\, k_f}{\phi(\mathbf{X}_{\mathrm{AB}}^{ij})} \Delta t \sum_{i=1}^{n_{\mathrm{A}}} m_{\mathrm{A}}^{i}\, W\left(\mathbf{X}_{\mathrm{A}}^{i} - \mathbf{X}_{\mathrm{B}}^{j}; \mathbf{H}_{\mathrm{A}} + \mathbf{H}_{\mathrm{B}}\right). \#(23)$$

In the particular one-dimensional case where only one particle of each reactant is present, porosity ϕ is constant in space, $\alpha = \beta = 1$, $H_{\mathrm{A}} = H_{\mathrm{B}} = h^2$, and all particles share the same mass *m*, we have

$$P(\mathrm{A} \rightarrow \mathrm{C}, \Delta t) = P(\mathrm{B} \rightarrow \mathrm{C}, \Delta t) = \frac{k_f}{\phi} \Delta t\; m\; \frac{1}{\sqrt{4\pi h^2}} \exp\left(-\frac{(x_{\mathrm{A}} - x_{\mathrm{B}})^2}{4h^2}\right), \#(24)$$

and we directly recover the probability of reaction between two isolated particles obtained by *Benson and Meerschaert* [2008]. We note that h in (24) is not $h = \sqrt{2D\Delta t}$ but rather it is defined as an optimal kernel support that changes with time according to the number of particles remaining and the actual shape of the solute plume. We claim that this difference in the definition of h is very significant. *Benson and Meerschaert* [2008] simulate incomplete mixing by using a low number of uniform- randomly distributed particles, which limits the reaction rate after some time as the A-particles

become isolated from the B-particles (described by the authors as "islands of particles"). Along the same line, *Paster et al.* [2013, 2014] derive a relationship between the initial particle density and the noise of the initial condition, suggesting that the simulation of smoother initial conditions requires a higher number of particles. In contrast, *Rahbalaram et al.* [2015] show that using the adaptive kernel makes it possible to highly reduce the dependence of the numerical solution on the number of particles. Another important difference between the two approaches becomes evident when more than one particle of each reactant is present. In this case, the probability of reaction of a particle given by (22) or (23) can be seen as the sum of independent particle pair interactions. This is only satisfied by the particle pair annihilation method in the limit when $\Delta t \to 0$. Otherwise, the reaction between two particles is not a disjoint event. Section 4 provides the details of the new particle tracking algorithm.

3. Extension to kinetic reactions with arbitrary reaction rate laws

The challenge in extending second-order reactions to arbitrary reaction rate laws resides in that now the total reaction rate cannot be simply split into combinations of kernel functions between particle pairs. Consequently, the rate at which two particles react depends also on all other surrounding particles. In this case, without any loss of generality, it is convenient to represent the total reaction rate as the product of a second-order reaction times g, a function of any arbitrary shape involving the reactants' concentrations, and denoted as compensation function,

$$r(\mathbf{x},t) = k_f c_{\mathrm{A}}(\mathbf{x},t) c_{\mathrm{B}}(\mathbf{x},t)\; g\big(c_{\mathrm{A}}(\mathbf{x},t), c_{\mathrm{B}}(\mathbf{x},t)\big). \#(25)$$

Applying $g = 1$ implies recovering (1). Substituting (5) into (25), and then decomposing as in (14) and substituting into (11) and (12), we now have,

357

$$P\left(\mathrm{A}^i \rightarrow \mathrm{C}^k, \Delta t\right) =$$

$$\frac{\alpha\, k_f}{\phi(\mathbf{X}_{\mathrm{AB}}^{ij})} \Delta t \sum_{j=1}^{n_{\mathrm{B}}} m_{\mathrm{B}}^j\, W\left(\mathbf{X}_{\mathrm{A}}^i - \mathbf{X}_{\mathrm{B}}^j; \mathbf{H}_{\mathrm{A}} + \mathbf{H}_{\mathrm{B}}\right) \int_{\Omega^d} W\left(\mathbf{x} - \mathbf{X}_{\mathrm{AB}}^{ij}; \mathbf{H}_{\mathrm{AB}}\right) g\left(c_{\mathrm{A}}(\mathbf{x}, t), c_{\mathrm{B}}(\mathbf{x}, t)\right) d\mathbf{x}, \#(26)$$

358

$$P\left(\mathrm{B}^j \rightarrow \mathrm{C}^k, \Delta t\right) =$$

$$\frac{\beta\, k_f}{\phi(\mathbf{X}_{\mathrm{AB}}^{ij})} \Delta t \sum_{j=1}^{n_{\mathrm{A}}} m_{\mathrm{A}}^j\, W\left(\mathbf{X}_{\mathrm{A}}^i - \mathbf{X}_{\mathrm{B}}^j; \mathbf{H}_{\mathrm{A}} + \mathbf{H}_{\mathrm{B}}\right) \int_{\Omega^d} W\left(\mathbf{x} - \mathbf{X}_{\mathrm{AB}}^{ij}; \mathbf{H}_{\mathrm{AB}}\right) g\left(c_{\mathrm{A}}(\mathbf{x}, t), c_{\mathrm{B}}(\mathbf{x}, t)\right) d\mathbf{x}, \#(27)$$

359

360 Because the compensation function $g(\mathbf{x}, t)$ depends on $\mathbf{x}$ in a complex manner, the
361 integration of (26) and (27) is no longer direct. To overcome this problem, we
362 approximate this integral by localizing the function $g(\mathbf{x}, t)$ about the point $\mathbf{x} = \mathbf{X}_{\mathrm{AB}}^{ij}$,
363 i.e., at the centroid of the kernel product (see figure 1), using a truncated first-order
364 Taylor series expansion (i.e., linearizing it in terms of location),

$$g(\mathbf{x}, t) \cong g\left(\mathbf{X}_{\mathrm{AB}}^{ij}, t\right) + \nabla g\left(\mathbf{X}_{\mathrm{AB}}^{ij}, t\right)^T \left(\mathbf{x} - \mathbf{X}_{\mathrm{AB}}^{ij}\right) \#(28)$$

365 The validity of this approximation is subjected to the significance of higher order terms
366 of g over the kernel product domain represented by $\mathbf{H}_{\mathrm{AB}}$. Note that the truncation error
367 will always converge towards zero with an increasing number of particles, namely, as
368 $\mathbf{H}_{\mathrm{AB}}$ approaches the Dirac delta. Introducing (28) into (26) and (27), and given that the
369 first moment of the kernel about its centroid equals zero, we obtain

$$P\left(\mathrm{A}^i \rightarrow \mathrm{C}^k, \Delta t\right) =$$

$$\frac{\alpha\, k_f}{\phi(\mathbf{X}_{AB}^{ij})} \Delta t \sum_{j=1}^{n_B} m_{\mathrm{B}}^j\, W\left(\mathbf{X}_A^i - \mathbf{X}_B^j; \mathbf{H}_A + \mathbf{H}_B\right) g\left(c_A\left(\mathbf{X}_{AB}^{ij}, t\right), c_B\left(\mathbf{X}_{AB}^{ij}, t\right)\right), \#(29)$$

$$P\left(B^j \rightarrow C^k, \Delta t\right) =$$

$$\frac{\beta\, k_f}{\phi(\mathbf{X}_{AB}^{ij})} \Delta t \sum_{i=1}^{n_A} m_A^i\, W\left(\mathbf{X}_A^i - \mathbf{X}_B^j; \mathbf{H}_A + \mathbf{H}_B\right) g\left(c_A\left(\mathbf{X}_{AB}^{ij}, t\right), c_B\left(\mathbf{X}_{AB}^{ij}, t\right)\right). \#(30)$$

The evaluation of $g\left(c_{\mathrm{A}}\left(\mathbf{X}_{\mathrm{AB}}^{ij}, t\right), c_{\mathrm{B}}\left(\mathbf{X}_{\mathrm{AB}}^{ij}, t\right)\right)$ in (29) and (30) requires an approximate solution of the concentrations of the species A and B at the specific location $\mathbf{X}_{\mathrm{AB}}^{ij}$. One possibility is to estimate these concentrations directly using the kernel estimator given in (5). However, this would require an excessive amount of calculations. To minimize CPU time, here we estimated these concentrations as a linear interpolation of the concentrations obtained only at the particle positions, estimated a priori by (5). This is possible as long as $\mathbf{X}_{\mathrm{A}}$, $\mathbf{X}_{\mathrm{AB}}$ and $\mathbf{X}_{\mathrm{B}}$ are aligned, i.e., $\mathbf{H}_{\mathrm{A}}$ and $\mathbf{H}_{\mathrm{B}}$ are isotropic, a condition that is inherently true in one dimension. This approach constitutes a simplification, and therefore it introduces some error in the solution. In the subsequent sections, we show that this error is small for a relatively low number of particles injected.

In the case where the reaction is reversible, it can be solved by combination of a forward and a backward reaction probability [*Benson and Meerschaert*, 2008]. For example, if the backward reaction is a first-order decay, i.e.,

$$\frac{1}{\gamma}\frac{dc_{\mathrm{C}}}{dt} = k_f\, c_{\mathrm{A}}(\mathbf{x}, t)\, c_{\mathrm{B}}(\mathbf{x}, t) - k_b c_{\mathrm{C}}(\mathbf{x}, t), \#(31)$$

where k_b is the backward reaction coefficient, then the probability of backward reaction is simply,

$$P\left(\mathrm{C}^k \rightarrow \mathrm{A}^i + B^j, \Delta t\right) = \gamma\, k_b\, \Delta t, \#(32)$$

and the mass of the disappearing particle C^k has to be distributed between the generated particles A^i and B^j in proportion to their stoichiometric coefficients. This, just like the separate treatment of transport and reaction described in the following section, constitutes a split operator approach, which implies that the time step Δt should not be too large in order to avoid error and instabilities.

Expressions (29) and (30) were derived under the assumption that particles are not at close distance from the domain boundaries. Should this condition not be fulfilled, different methods exist in the literature to make KDE valid near domain boundaries. A simple one, in principle only valid for regular boundaries, is the reflection method [*Silverman*, 1986]: for every particle that is at close distance from a boundary (beneath some significance threshold) an identical virtual particle is placed as a reflection on the other side of that boundary. This complies with mass conservation inside the domain ($\int_{\Omega^d} c_s(\mathbf{x}, t)\, d\mathbf{x} = \sum_{i=1}^{n_s} m_s^i$), and also imposes a zero-gradient boundary condition. Then, the methodology that we describe in this paper can be used as long as the virtual particles are considered in the computation of the right hand side of (29) and/or (30).

4. The random walk algorithm

In the proposed method, reactive transport is solved in two stages, one corresponding to the chemical reactions, and another one to the standard advection-dispersion equation. This split operator approach is known in the literature as RT [*Simpson and Landman*, 2007]. Of course, other split operator approaches could also be implemented in a similar way. *Morshed and Kaluarachchi* [1995] show that operator splitting in non-linear reactive transport can have significant restrictions on the time step size to obtain

411 accurate solutions. *Simpson and Landman* [2007] show that the error associated to
412 operator splitting can be removed by using an alternating scheme provided Δt is
413 sufficiently small. *Paster et al.* [2014] derive some practical criteria for the selection of
414 the time step in a Lagrangian model of reactive transport with second order kinetics. In
415 this work, the time step was simply chosen small enough in each example to reach
416 convergence of the solution. Alternatively, an adapted time step can be estimated by
417 fixing the maximum probability of reaction. This way, the time step is respectively
418 small or large at stages where the reaction is fast or slow.

419

420 The procedure used in this work to simulate kinetic reactions based on the probabilities
421 determined by (29) can be written as it follows: First, for each time step Δt, the
422 probability of reaction of only one of the reactants (A or B) is estimated. For simplicity,
423 and without any loss of generality, we will assume it to be the reactant A. Then, a
424 uniform [0, 1] random number μ is drawn for each A-particle and compared to the
425 corresponding probability of reaction, $P\left(\mathrm{A}^i \rightarrow \mathrm{C}^k, \Delta t\right)$. If $\mu \leq P\left(\mathrm{A}^i \rightarrow \mathrm{C}^k, \Delta t\right)$, it is
426 considered that particle A^i does not react and the algorithm continues with the next A-
427 particle. On the contrary, if $\mu > P\left(\mathrm{A}^i \rightarrow \mathrm{C}^k, \Delta t\right)$, the A-particle reacts with a number of
428 nearby B-particles (the closest ones). To satisfy stoichiometry, the number of B-
429 particles reacting with the A-particle, denoted here as n_r, is a positive integer value that
430 should fulfill the following expression,

$$\alpha \sum_{j=1}^{n_r} m_{\mathrm{B}}^j = \beta \, m_{\mathrm{A}}^i . \#(33)$$

431 When the reaction occurs, one C-particle is injected at each $\mathbf{X}_{\mathrm{AB}}^{ij}$ position located
432 between the reacting particle pairs $\{\mathrm{A}^i, \mathrm{B}^j\}$. These reacting particle pairs disappear after

433 that. Again, by stoichiometry, the mass associated with each new C-particle should
434 fulfill that

$$\sum_{k=1}^{n_r} m_{\mathrm{C}}^{k} = \frac{\gamma}{\alpha+\beta}\left(m_{\mathrm{A}}^{i} + \sum_{j=1}^{n_r} m_{\mathrm{B}}^{j} \right). \#(34)$$

435 If all particles associated with a given species share a constant mass, these expressions
436 reduce to the following simple relationships,

$$\frac{m_{\mathrm{A}}}{m_{\mathrm{B}}} = \frac{\alpha}{\beta}\, n_r, \#(35)$$

$$m_{\mathrm{C}} = \frac{\gamma}{\beta}\, m_{\mathrm{B}}. \#(36)$$

437 To satisfy (35) when n_r is a real value, this expression simply requires to slightly
438 modify the particle mass associated with the reactants prior to the beginning of the
439 simulation. In the case of an instantaneous injection or to reproduce an initial condition,
440 this will imply choosing an adequate ratio between the number of particles of each
441 reactant. A valid alternative, not implemented in this work although perfectly
442 compatible with the presented method, is to change the particle mass upon reaction
443 [*Bolster et al*., 2016], using (9) and (10) to determine the particle mass variation from
444 the computed probability. Another alternative is to decide the reaction of particle pairs
445 $\{\mathrm{A}, \mathrm{B}\}$ based on Bernoulli trials with a probability of failure determined by $f = n_r -$
446 $F(n_r)$. Here, $F(x)$ is the floor function defined as the greatest integer less than or equal
447 to x. However, in this case, stoichiometry is only fulfilled in an average sense. The
448 latter approach is used in Example 1.

449

After this, following the standard random walk method, each particle is moved according to a drift term and a Brownian motion to respectively simulate advection and dispersion,

$$\mathbf{X}_s^i(t+\Delta t) = \mathbf{X}_s^i(t) + \mathbf{v}_s\left(\mathbf{X}_s^i(t)\right)\,\Delta t + \mathbf{E}_s\left(\mathbf{X}_s^i(t)\right)\boldsymbol{\xi}\sqrt{\Delta t}, \#(37)$$

where $\mathbf{X}_s^i(t)$ is the *i*th particle position associated with species s, $\mathbf{v}_s$ is the particle velocity associated with species s given by $\mathbf{v}_s = \frac{\mathbf{q}}{\phi R_s} + \frac{1}{\phi R_s}\nabla\cdot(\phi\mathbf{D}_s)$, R_s is the retardation factor associated with species s, $\mathbf{D}_s$ is the local hydrodynamic dispersion tensor associated with species s, $\mathbf{E}_s$ is the Brownian displacement matrix determined by $\mathbf{E}_s\mathbf{E}_s^T = 2\mathbf{D}_s/R_s$, and $\boldsymbol{\xi}$ is a vector of d standard normally distributed random numbers. Note that the method can directly support species-dependent properties such as effective particle velocity (affected by retardation) and dispersion. Note also that alternative equations to the advection-dispersion could be used in this step (e.g., Continuous Time Random Walks), as the processes of transport and reaction are fully decoupled.

5. Performance and convergence of the method

Four simple hypothetical case examples were solved using the proposed methodology to evaluate the performance and convergence of the method as a function of the number of injected particles. The selected problems illustrate a wide range of possible applications. For each problem, we simulate reactive transport in a one-dimensional column of unit ($1\ \mathrm{m}^2$) cross-section, with constant velocity, porosity, and dispersion, to emphasize only the relevance of the complex reactions. The parameter values adopted in each example are given in tables 1-4.

472 Simulations are performed in a Monte Carlo framework consisting of 100 random walk
473 particle tracking realizations. Results are compared with those obtained from a very
474 finely discretized finite difference solver for the ADRE with explicit time stepping and
475 upwind differences in space for the advection term, which was checked for spatial and
476 temporal convergence. The finite difference solution is assumed to represent the true
477 solution. As explained in the previous section and although other approaches could be
478 used, we assigned equal mass to all particles belonging to the same species so that
479 stoichiometry is fulfilled exactly. Whenever possible, we imposed that the ratio of the
480 reactant masses matches that of the stoichiometric coefficients, i.e., $n_r = 1$ in (35). The
481 method was implemented in a Random Walk Particle Tracking code written in Matlab.
482 At the start of each simulation, 5000 particles of each reactant were injected following
483 Gaussian distributions in space characterized by the mean, the standard deviation and
484 the total amount of substance indicated in tables 1-4. In all cases, the concentration of
485 all compounds in the inflow is zero at all times.

486

487 The support of each species was estimated through (7) by assuming a Gaussian shape of
488 the particle plume. This leads to a suboptimal approximation of the particle support
489 volume written as [e.g. *Silverman*, 1986],

$$h_s = 1.06\, \sigma_{x,s}\, n_s^{-\frac{1}{5}}, \#(38)$$

490 where the index *s* denotes the chemical species, n_s is the number of particles of the *s*th
491 species, and $\sigma_{x,s}$ is the standard deviation of the particle positions of the *s*th species at a
492 given time.

493

494 **5.1. Description of the chemical systems**

Example 1. A Generic reaction with fractional exponents

In this first example, we consider a generic kinetic reaction with arbitrary stoichiometric coefficients, $\alpha\ \mathrm{A} + \beta\ \mathrm{B} \rightarrow \gamma\ \mathrm{C}$. The reaction rate is written as

$$r(x,t) = k_f\ c_\mathrm{A} c_\mathrm{B}\ g(c_\mathrm{A}, c_\mathrm{B}), \#(39)$$

where the compensation function *g* in this case is

$$g(c_\mathrm{A}, c_\mathrm{B}) = c_\mathrm{A}^{\theta_\mathrm{A}-1}\ c_\mathrm{B}^{\theta_\mathrm{B}-1}. \#(40)$$

Here, θ_A and θ_B are arbitrary real values, often (but not always) associated with the stoichiometric coefficients. To illustrate that any reaction with fractional exponents can be properly simulated, we chose $\theta_\mathrm{A} = \alpha = 2.3$ and $\theta_\mathrm{B} = \beta = 1.3$. The parameters adopted during the simulations are summarized in Table 1.

Example 2. Aerobic Michaelis-Menten degradation considering linear sorption of organic carbon

In this example we reproduce the aerobic biodegradation of an organic chemical compound dissolved in groundwater. The organic compound ($\mathrm{CH_2O}$) is subject to linear sorption, with a retardation factor $R = 3$. Microbial growth and decay is neglected, and the dissolved organic carbon is assumed to react with dissolved oxygen to form carbon dioxide and water, $\mathrm{CH_2O + O_2 \rightarrow CO_2 + H_2O}$. The reaction rate follows the Michaelis-Menten kinetic model written here as

$$r(x,t) = k_f\ c_{\mathrm{CH_2O}}\ c_{\mathrm{O_2}}\ g\left(c_{\mathrm{CH_2O}}, c_{\mathrm{O_2}}\right), \#(41)$$

with function *g* being defined in this case as

$$g\left(c_{\mathrm{CH_2O}}, c_{\mathrm{O_2}}\right) = \frac{1}{k_{\mathrm{CH_2O}} + c_{\mathrm{CH_2O}}}\ \frac{1}{k_{\mathrm{O_2}} + c_{\mathrm{O_2}}}. \#(42)$$

513 k_{CH_2O} and k_{O_2} are the half-saturation constants associated with the dissolved organic
514 carbon and oxygen, respectively.

515

516 The plume of oxygen rapidly migrates towards the organic chemical compound with an
517 effective retardation of $R = 1$. We assumed that the carbon dioxide produced by the
518 chemical reaction remains dissolved in groundwater as $CO_{2\,(aq)}$. The degradation
519 constant value and the half-saturation constant values are taken from *Rolle et al*. [2008]
520 and *Nagy et al.* [2009]. The parameters adopted during the simulations are summarized
521 in Table 2.

522

523 **Example 3. Calcite precipitation**

524 This example simulates the precipitation of calcium carbonate that takes place at the
525 contact fringe of two moving solute plumes of Ca^{2+} and CO_3^{2-}. Remarkably, we
526 consider the effect of the nontrivial activity coefficients involved in the chemical
527 reaction. We neglect the changes in the hydraulic properties of the porous medium
528 resulting from precipitation. Back-dissolution is also omitted. The chemical reaction is
529 formally written as $Ca^{2+} + CO_3^{2-} \rightarrow CaCO_{3(s)}$. The rate of precipitation is represented
530 by [e.g., *Nancollas*, 1979],

$$r(x,t) = k_{obs}(\Omega - 1), \#(43)$$

531 where k_{obs} is an observed or effective rate constant and Ω is the saturation state. We can
532 rewrite this expression as:

$$r(x,t) = k' c_{Ca^{2+}}\, c_{CO_3^{2-}} \left(\gamma_{Ca^{2+}}\, \gamma_{CO_3^{2-}} - \frac{k_{eq}}{c_{Ca^{2+}}\, c_{CO_3^{2-}}} \right). \#(44)$$

Here, $\gamma_{Ca^{2+}}$, $\gamma_{CO_3^{2-}}$ are the activity coefficients of Ca^{2+} and CO_3^{2-}, respectively, k_{eq} is the equilibrium or solubility constant, and $k' = k_{obs}/k_{eq}$. From this, the compensation function associated with this chemical reaction is expressed as

$$g(\mathrm{c}_{\mathrm{Ca}^{2+}}, \mathrm{c}_{\mathrm{CO}_3^{2-}}) = \gamma_{Ca^{2+}}\,\gamma_{CO_3^{2-}} - \frac{k_{eq}}{\mathrm{c}_{\mathrm{Ca}^{2+}}\,\mathrm{c}_{\mathrm{CO}_3^{2-}}}. \#(45)$$

We assume that Ca^{2+} and CO_3^{2-} are the only ions with significant concentrations in the solution. Then, by using the extended Debye-Hückel formula, the activity coefficients $\gamma_{\mathrm{Ca}^{2+}}\,\gamma_{\mathrm{CO}_3^{2-}}$ are calculated as,

$$\log_{10}(\gamma_{\mathrm{Ca}^{2+}}\,\gamma_{\mathrm{CO}_3^{2-}}) = -4k_1\left(\frac{1}{\frac{1}{\sqrt{2(\mathrm{c}_{\mathrm{Ca}^{2+}} + \mathrm{c}_{\mathrm{CO}_3^{2-}})}} + k_2\,\mathring{a}_{\mathrm{Ca}^{2+}}} + \frac{1}{\frac{1}{\sqrt{2(\mathrm{c}_{\mathrm{Ca}^{2+}} + \mathrm{c}_{\mathrm{CO}_3^{2-}})}} + k_2\,\mathring{a}_{\mathrm{CO}_3^{2-}}}\right), \#(46)$$

where $k_1 = 0.018846\ \mathrm{m}^{3/2}/\mathrm{mol}^{1/2}$ and $k_2 = 0.103755\ \mathrm{m}^{3/2}/\mathrm{mol}^{1/2}\,nm$ for water at 25ºC (assuming that the density of water is $\rho_w = 1\ \mathrm{Kg/dm}^3$), and $\mathring{a}_{\mathrm{Ca}^{2+}}$, $\mathring{a}_{\mathrm{CO}_3^{2-}}$ are the hydrated radii of the respective ions [*Garrels and Christ*, 1965]. Values for k_{obs}, k_{eq} were taken from *van Breukelen* [2003] and *Appelo and Postma* [2005], respectively. The parameters adopted during the simulations are summarized in Table 3.

Example 4. Acidic dissolution of Fluorite:

This example describes the acidic dissolution of fluorite. The chemical reaction is $\mathrm{CaF}_2 + 2\mathrm{H}^+ \rightarrow \mathrm{Ca}^{2+} + 2\mathrm{HF}^0$, and the dissolution rate is typically represented by [*Zhang et al*., 2006],

$$r(x,t) = k\,S_s\,(c_{\mathrm{H}^+}^2/c_{\mathrm{Ca}^{2+}})^{\alpha}, \#(47)$$

549 Where S_s is the mineral (CaF_2) surface per cubic meter of the porous medium, and k
550 and α are experimental parameters. Zhang and coworkers found that at 25ºC $\log k$
551 ranged approximately between -2 and -4 for different experimental conditions,
552 whereas α had values between 0.495 and 1.146. Here, we chose $\log k = -4$ and
553 $\alpha = 0.8$, so that

$$r(x,t) = k\, S_s\, c_{H^+}^{\theta_{H^+}}\, c_{Ca^{2+}}^{\theta_{Ca^{2+}}}, \#(48)$$

554 where $\theta_{H^+} = 1.6$ and $\theta_{Ca^{2+}} = -0.8$. This kinetic model resembles that of the example
555 1, but with the presence of a negative exponent in the concentration of Ca^{2+}. We
556 consider that Fluorite is everywhere in the system and in high amounts, and so S_s is a
557 constant. Then the model has only one reactant and two products, although one of the
558 products has an influence on the reaction rate. This means that, for this particular case,
559 injection of the product particles is performed directly on the position of the reacting
560 particle. We neglect the changes in the hydraulic properties of the porous medium
561 resulting from dissolution. The chemical reaction can be embedded in (24) by defining
562 that

$$g(c_{H^+}, c_{Ca^{2+}}) = c_{H^+}^{\theta_{H^+}-1}\, c_{Ca^{2+}}^{\theta_{Ca^{2+}}-1}, \#(49)$$

563 and $k\, S_s = k_f$. In this case, two overlapping plumes of H^+ and Ca^{2+} are injected at the
564 same initial location (note that the reaction rate has an asymptote in case of total
565 absence of Ca^{2+}). The parameters adopted during the simulations are summarized in
566 Table 4.

567

568 **5.2. Results**

569 Figures 2-9 compare the random walk solution obtained at the end of the simulation
570 time with the corresponding finite difference solution for each reactive transport
571 problem. The random walk solution is presented in terms of the mean concentration of
572 the different chemical species and its standard deviation (the shaded zone delimits ±1
573 standard deviation) obtained from 100 realizations. For completeness, the corresponding
574 evolution of the total mass of the different chemical species remaining in the column
575 during the simulation are also depicted in these figures. Considering that the reactive
576 transport problems were simulated with only 5000 particles, a good match is obtained
577 for all cases.

578

579 We note that larger deviations from the finite difference solution can be seen at the
580 concentration peaks. This is mostly attributed to the fact that the suboptimal
581 approximation of the particle support volume directly affects the calculation of the
582 probabilities in (29) through the estimation of concentrations in the compensation
583 function g. This effect is seen most significant when g deviates from zero-order
584 (corresponding to second-order kinetic reactions, where there is no need for
585 compensation).

586

587 The approximation (38) used to determine the particle support volume h_s is only valid
588 for Gaussian distributions of the species' concentrations. This is particularly not
589 satisfied for calcium ion in the acidic dissolution of Fluorite (see Figure 8). Hence,
590 errors in the estimation of the resulting concentration map in this case example are
591 slightly larger than in the others. In practice, the use of such an approximation of h_s
592 (known as the rule-of-thumb in statistics), implies that more particles are needed to

match the exact solution. Yet, the use of (7) may become computationally expensive in reactive transport problems otherwise.

Figure 10 shows the average relative error (ϵ_r) and the coefficient of variation (CV_r) of the increase in the total amount of substance at the end of the simulation, calculated over 100 realizations by comparison with the finite difference solution,

$$\epsilon_r = \frac{\langle M_{PT} \rangle - M_{FD}}{\Delta M_{FD}}, \#(50)$$

$$CV_r = \frac{\sqrt{\langle {M_{PT}}^2 \rangle - \langle M_{PT} \rangle^2}}{|\Delta M_{FD}|}, \#(51)$$

where M_{PT} is the total mass of a given chemical compound obtained at the final simulation time, $\langle \cdot \rangle$ is the mean operator over all realizations, M_{FD} is the total mass of the chemical compound obtained with finite difference at the end of the simulation time, and ΔM_{FD} is the total mass variation of the chemical compound obtained with the finite difference method. The mean relative error ϵ_r represents the systematic error associated to one realisation, whereas CV_r accounts for its random variability. Note that the sum of the squares of these two parameters is the Mean Squared Error (MSE) of ΔM_{PT}, normalized by ${\Delta M_{FD}}^2$. Results show that the proposed random walk method converges towards the exact solution with an increasing number of particles. It also demonstrates that not many particles are needed to simulate non-linear chemical reactions with sufficient accuracy.

6. Importance of chemical kinetics in heterogeneous aquifers: An example

A two-dimensional implementation of the proposed method in a heterogeneous aquifer is given in this section. The objective of this example is to illustrate the application of

613 the presented random walk approach in a more realistic setting. In doing this, we
614 analyze the need of fully describing non-linear chemical kinetics in heterogeneous
615 porous media.

616 We study a reactive transport problem in a 2D rectangular confined aquifer with
617 dimensions of 100×50 m^2. The aquifer is characterized by a randomly generated log-
618 normally distributed hydraulic conductivity field $Y = \ln K$ with a mean of $\langle Y \rangle = 3$ and
619 a variance of $\sigma_Y^2 = 1$. The Y field follows an isotropic exponential covariance function
620 model with integral scale of $I_Y = 5$ m. The other aquifer properties are assumed
621 homogeneous. Groundwater flow is considered at steady-state and subject to constant
622 head conditions at the lateral boundaries and impermeable conditions otherwise. As a
623 result, the mean flow direction is oriented in the x-direction and characterized by a
624 mean hydraulic gradient of 0.00622. The flow problem is solved with a finite-difference
625 code, MODFLOW-2000 [*Harbaugh et al*., 2000], with a domain discretized into regular
626 cells of size 0.5 m. The resulting cell face flows were used to compute the random walk
627 particle velocities according to the hybrid interpolation method suggested by *LaBolle et*
628 *al.* [1996].

629 The reactive transport problem is similar to the one defined in example 2 but considers a
630 two-dimensional heterogeneous porous media. A schematic representation of the system
631 is shown in Figure 11. A plume of dissolved organic matter, retarded with respect to
632 groundwater by linear sorption, passes after some time through an oxygen plume. The
633 chemical reaction follows the Michaelis-Menten kinetic model with the same
634 formulation and parameter values as given in example 2. Table 2 shows the values of
635 the parameters. The concentrations of the reactants are initially uniform in two separate
636 rectangular areas depicted in Figure 11 and zero everywhere else in the domain. The
637 concentration of all compounds in the inflow water is zero at all times.

638 The fast method of *Botev et al.* [2010] was used to determine the kernel bandwidth with
639 a slight modification: the anisotropic kernel bandwidth matrix $\boldsymbol{H}$ obtained by this
640 method was transformed into an isotropic bandwidth by matching the determinants, i.e.,
641 $h^2 = \det(\boldsymbol{H})$. As explained in section 3, the use of isotropic kernels facilitates the
642 computation of the compensation function g at the $\mathbf{X}_{AB}^{ij}$ location by linear interpolation.
643 However, the kernel obtained by this approach is suboptimal compared to the original
644 method by *Botev et al.* [2010], and presumably produced a slower convergence with
645 respect to the number of particles.

646 The convergence of the random walk solution was controlled by choosing a small
647 enough time step and by performing a sensitivity analysis with respect to the number of
648 particles. As expected, the convergence occurred for a higher number of particles
649 compared to the 1D examples. Nevertheless, by using only 32,768 particles of each
650 reactant, the estimated error in the total amount of product generated was below 1% as
651 compared to the solution obtained with 131,072 particles. Figure 12 shows the three
652 particle plumes at different moments of the simulation (for a better visualization, only a
653 random subsample of 5,000 particles is shown), and the corresponding KDE
654 reconstruction of the product concentrations.

655

656 The actual impact of the reaction kinetics on the problem solution depends on whether
657 mixing or chemical kinetics is the limiting process. In order to illustrate this, we
658 compare the evolution of the CO_2 production with the following equivalent second-
659 order reaction,

$$r(\mathbf{x}, t) = \frac{k_f}{k_{\mathrm{CH_2O}}\, k_{\mathrm{O_2}}}\, c_{\mathrm{CH_2O}}\, c_{\mathrm{O_2}},$$

660 for three different values of k_f ranging from five times smaller to five times higher than
661 the value given in Table 2. Figure 13 shows that for a very fast reaction rate the process
662 is mixing-limited (in this case mixing is driven by the difference in the retardation
663 coefficients), and therefore the reaction kinetics do not have a significant effect on the
664 results. These kind of reactions can be modeled as instantaneous (ref. xavi), as long as
665 the mixing process is well represented by the transport model. On the other hand, in
666 slow reactions, the reaction kinetics can make a very important difference in the results.

667 ## 7. Conclusions

668 We have presented a new random walk particle tracking method to simulate reactions
669 with complex kinetics involving two reactants. Reactive transport is solved in two
670 stages: the first one corresponding to the chemical reactions, and the second one to the
671 standard advection-dispersion equation. The method is based on the representation of
672 particles by optimal kernel functions. This way, we derived the probability that a given
673 particle reacts with any particle associated with other reactants. In the proposed
674 methodology, complex kinetic reactions require linearizing a function of the local
675 concentrations at the location of highest probability density of encounter between
676 potentially reactive particle pairs. The implementation of the probability of reaction in
677 random walk models has been achieved in this paper by particle annihilation, but other
678 approaches such as particle mass variations can easily be incorporated.

679

680 In addition, two simple relationships should be satisfied to fulfill stoichiometry: one
681 relating the mass of interacting particles with the stoichiometric coefficients, and
682 another one relating the mass of particles produced from reactions with the
683 stoichiometric coefficients. In practice, the first relationship requires a careful choice of

684 the mass of the particles injected. The second relationship determines the mass of
685 particles produced from the chemical reaction.

686

687 Several synthetic examples demonstrate the potential applicability of the method in a
688 wide range of applications, ranging from reaction-rate laws with fractional exponents to
689 acidic dissolution and precipitation systems with nontrivial activity coefficients. Results
690 have shown that a good match with a finite difference solution is obtained with
691 relatively few particles. The method has been demonstrated to converge to the solution
692 with an increasing number of particles. This rate of convergence depends on the type of
693 chemical reaction, i.e., on the shape of the compensation function *g*. Finally, a 2D
694 example dealing with non-linear Michaelis-Menten biodegradation in a randomly
695 heterogeneous aquifer is provided to illustrate the capabilities of the method in a more
696 realistic setting.

697

698

699 **Acknowledgements**

700 Financial support was provided by the Spanish Government, through projects WE-
701 NEED, PCIN-2015-248; ACWAPUR, PCIN-2015-239, and INDEMNE, CGL2015-
702 69768-R (MINECO/FEDER). GS acknowledges financial support by AGAUR. The
703 paper provides all the information needed to replicate the results. The codes and the
704 output data from the simulations are freely available from the authors upon request.

705 **References**

706 Andricevic, R., and E. Foufoula-Georgiou (1991), Modeling kinetic non-equilibrium
707 using the first two moments of the residence time distribution, *Stoch. Hydrol.*
708 *Hydraul.*, *5*(2), 155–171, doi:10.1007/BF01543057.

709 Appelo, C. A. J., and D. Postma (2006), Geochemistry, Groundwater and Pollution,
710 *Vadose Zo. J.*, *5*(1), 510, doi:10.2136/vzj2005.1110br.

711 Benson, D. A., T. Aquino, D. Bolster, N. Engdahl, C. V. Henri, and D. Fernàndez-
712 Garcia (2017), A comparison of Eulerian and Lagrangian transport and non-linear
713 reaction algorithms, *Adv. Water Resour.*, *99*, 15–37,
714 doi:10.1016/j.advwatres.2016.11.003.

715 Benson, D. A., and D. Bolster (2016), Arbitrarily complex chemical reactions on
716 particles, *Water Resour. Res.*, *52*(11), 9190–9200, doi:10.1002/2016WR019368.

717 Benson, D. A., and M. M. Meerschaert (2009), A simple and efficient random walk
718 solution of multi-rate mobile/immobile mass transport equations, *Adv. Water*
719 *Resour.*, *32*(4), 532–539, doi:10.1016/j.advwatres.2009.01.002.

720 Benson, D. A., and M. M. Meerschaert (2008), Simulation of chemical reaction via
721 particle tracking: Diffusion-limited versus thermodynamic rate-limited regimes,
722 *Water Resour. Res.*, *44*(12), n/a-n/a, doi:10.1029/2008WR007111.

723 Berkowitz, B., A. Cortis, M. Dentz, and H. Scher (2006), Modeling Non-fickian
724 transport in geological formations as a continuous time random walk, *Rev.*
725 *Geophys.*, *44*(2), doi:10.1029/2005RG000178.

726 Bolster, D., A. Paster, and D. A. Benson (2016), A particle number conserving
727 Lagrangian method for mixing-driven reactive transport, *Water Resour. Res.*,
728 *52*(2), 1518–1527, doi:10.1002/2015WR018310.

729 Cui, Z., C. Welty, and R. M. Maxwell (2014), Modeling nitrogen transport and
730 transformation in aquifers using a particle-tracking approach, *Comput. Geosci.*, *70*,
731 1–14, doi:10.1016/j.cageo.2014.05.005.

732 Cvetkovic, V., and R. Haggerty (2002), Transport with multiple-rate exchange in
733 disordered media, *Phys. Rev. E - Stat. Nonlinear, Soft Matter Phys.*, *65*(5),
734 doi:10.1103/PhysRevE.65.051308.

735 De Simoni, M., X. Sanchez-Vila, J. Carrera, and M. W. Saaltink (2007), A mixing
736 ratios-based formulation for multicomponent reactive transport, *Water Resour.*
737 *Res.*, *43*(7), doi:10.1029/2006WR005256.

738 Delay, F., and J. Bodin (2001), Time domain random walk method to simulate transport
739 by advection-dispersion and matrix diffusion in fracture networks, *Geophys. Res.*
740 *Lett.*, *28*(21), 4051–4054, doi:10.1029/2001GL013698.

741 Dentz, M., and A. Castro (2009), Effective transport dynamics in porous media with
742 heterogeneous retardation properties, *Geophys. Res. Lett.*, *36*(3),
743 doi:10.1029/2008GL036846.

744 Ding, D., and D. A. Benson (2015), Simulating biodegradation under mixing-limited
745 conditions using Michaelis-Menten (Monod) kinetic expressions in a particle
746 tracking model, *Adv. Water Resour.*, *76*, 109–119,
747 doi:10.1016/j.advwatres.2014.12.007.

748 Ding, D., D. A. Benson, D. Fernàndez-Garcia, C. V. Henri, M. S. Phanikumar, and D.
749 W. Hyndman (2017), Elimination of the reaction “scale effect": Application of the
750 Lagrangian reactive particle-tracking method to simulate mixing-limited, field
751 scale biodegradation at the Schoolcraft, Michigan site., *Water Resour. Res.*, Under
752 review.

753 Engel, J., E. Herrmann, and T. Gasser (1994), An iterative bandwidth selector for kernel
754 estimation of densities and their derivatives, *J. Nonparametr. Stat.*, *4*(1), 21–34,
755 doi:10.1080/10485259408832598.

756 Fernàndez-Garcia, D., and X. Sanchez-Vila (2011), Optimal reconstruction of
757 concentrations, gradients and reaction rates from particle distributions, *J. Contam.*
758 *Hydrol.*, *120–121*(C), 99–114, doi:10.1016/j.jconhyd.2010.05.001.

759 Garrels, R. M., and C. L. Christ (1965), *Solutions, minerals, and equilibria*, New York:
760 Harper and Row.

761 Härdle, W. (1991), Kernel Density Estimation, in *Smoothing Techniques: With*
762 *Implementation in S*, pp. 43–84, Springer New York, New York, NY.

763 Henri, C. V., and D. Fernàndez-Garcia (2014), Toward efficiency in heterogeneous
764 multispecies reactive transport modeling: A particle-tracking solution for first-
765 order network reactions, *Water Resour. Res.*, *50*(9), 7206–7230,
766 doi:10.1002/2013WR014956.

767 Henri, C. V., and D. Fernàndez-Garcia (2015), A random walk solution for modeling
768 solute transport with network reactions and multi-rate mass transfer in
769 heterogeneous systems: Impact of biofilms, *Adv. Water Resour.*, *86*, 119–132,
770 doi:10.1016/j.advwatres.2015.09.028.

771 Huang, H., A. E. Hassan, and B. X. Hu (2003), Monte Carlo study of conservative
772 transport in heterogeneous dual-porosity media, in *Journal of Hydrology*, vol. 275,
773 pp. 229–241.

774 Kinzelbach, W. (1988), The Random Walk Method in Pollutant Transport Simulation,
775 in *Groundwater Flow and Quality Modelling*, edited by E. Custodio, A. Gurgui,
776 and J. P. L. Ferreira, pp. 227–245, Springer Netherlands, Dordrecht.

777 LaBolle, E. M., G. E. Fogg, and A. F. B. Tompson (1996), Random-walk simulation of
778 transport in heterogeneous porous media: Local mass-conservation problem and
779 implementation methods, *Water Resour. Res.*, *32*(3), 583–593,
780 doi:10.1029/95WR03528.

781 Michalak, A. M., and P. K. Kitanidis (2000), Macroscopic behavior and random-walk
782 particle tracking of kinetically sorbing solutes, *Water Resour. Res.*, *36*(8), 2133–
783 2146, doi:10.1029/2000WR900109.

784 Nagy, A. M., G. Mourot, B. Marx, G. Schutz, and J. Ragot (2009), Model structure
785 simplification of a biological reactor, *IFAC Proc. Vol.*, *42*(10), 257–262,
786 doi:10.3182/20090706-3-FR-2004.00043.

787 Nancollas, G. H. (1979), The growth of crystals in solution, *Adv. Colloid Interface Sci.*,
788 *10*(1), 215–252, doi:10.1016/0001-8686(79)87007-4.

789 Paster, A., D. Bolster, and D. A. Benson (2014), Connecting the dots: Semi-analytical
790 and random walk numerical solutions of the diffusion-reaction equation with
791 stochastic initial conditions, *J. Comput. Phys.*, *263*, 91–112,
792 doi:10.1016/j.jcp.2014.01.020.

793 Pedretti, D., and D. Fernàndez-Garcia (2013), An automatic locally-adaptive method to
794 estimate heavily-tailed breakthrough curves from particle distributions, *Adv. Water*
795 *Resour.*, *59*, 52–65, doi:10.1016/j.advwatres.2013.05.006.

796 Rahbaralam, M., D. Fernàndez-Garcia, and X. Sanchez-Vila (2015), Do we really need
797 a large number of particles to simulate bimolecular reactive transport with random
798 walk methods? A kernel density estimation approach, *J. Comput. Phys.*, *303*, 95–
799 104, doi:10.1016/j.jcp.2015.09.030.

800 Rahbaralam, M., D. Fernàndez-Garcia, 662 and X. Sanchez-Vila (2017), Modeling of
801 non-linear adsorption with particle tracking and kernel density estimators, *Water*
802 *Resour. Res.*, Under review.

803 Riva, M., A. Guadagnini, D. Fernandez-Garcia, X. Sanchez-Vila, and T. Ptak (2008),
804 Relative importance of geostatistical and transport models in describing heavily
805 tailed breakthrough curves at the Lauswiesen site, *J. Contam. Hydrol.*, *101*(1–4),
806 1–13, doi:10.1016/j.jconhyd.2008.07.004.

807 Salamon, P., D. Fernàndez-Garcia, and J. J. Gómez-Hernández (2007), Modeling tracer
808 transport at the MADE site: The importance of heterogeneity, *Water Resour. Res.*,
809 *43*(8), doi:10.1029/2006WR005522.

810 Salamon, P., D. Fernàndez-Garcia, and J. J. Gómez-Hernández (2006), Modeling mass
811 transfer processes using random walk particle tracking, *Water Resour. Res.*,
812 *42*(11), doi:10.1029/2006WR004927.

813 Salamon, P., D. Fernàndez-Garcia, and J. J. Gómez-Hernández (2006), A review and
814 numerical assessment of the random walk particle tracking method, *J. Contam.*
815 *Hydrol.*, *87*(3–4), 277–305, doi:10.1016/j.jconhyd.2006.05.005.

816 Sánchez-Vila, X., and J. Solís-Delfín (1999), Solute transport in heterogeneous media:
817 The impact of anisotropy and non-ergodicity in risk assessment, *Stoch. Environ.*
818 *Res. Risk Assess.*, *13*(5), 365–379, doi:10.1007/s004770050056.

819 Schmidt, M. J., S. Pankavich, and D. A. Benson (2017), A Kernel-based Lagrangian
820 method for imperfectly-mixed chemical reactions, *J. Comput. Phys.*, *336*, 288–307,
821 doi:10.1016/j.jcp.2017.02.012.

822 Siirila-Woodburn, E. R., D. Fernàndez-Garcia, and X. Sanchez-Vila (2015), Improving
823 the accuracy of risk prediction from particle-based breakthrough curves
824 reconstructed with kernel density estimators, *Water Resour. Res.*, *51*(6), 4574–
825 4591, doi:10.1002/2014WR016394.

826 Silverman, B. W. (1986), *Density Estimation for Statistics and Data Analysis*.

827 Simpson, M. J., and K. A. Landman (2007), Analysis of split operator methods applied
828 to reactive transport with Monod kinetics, *Adv. Water Resour.*, *30*(9), 2026–2033,
829 doi:10.1016/j.advwatres.2007.04.005.

830 Tompson, A. F. B. (1993), Numerical simulation of chemical migration in physically
831 and chemically heterogeneous porous media, *Water Resour. Res.*, *29*(11), 3709–
832 3726, doi:10.1029/93WR01526.

833 Tompson, A. F. B., and L. W. Gelhar (1990), Numerical simulation of solute transport
834 in three???dimensional, randomly heterogeneous porous media, *Water Resour.*
835 *Res.*, *26*(10), 2541–2562, doi:10.1029/WR026i010p02541.

836 Tompson, A. F. B., A. L. Schafer, and R. W. Smith (1996), Impacts of physical and
837 chemical heterogeneity on cocontaminant transport in a sandy porous medium,
838 *Water Resour. Res.*, *32*(4), 801–818, doi:10.1029/95WR03733.

839 Tsang, Y. W., and C. F. Tsang (2001), A particle-tracking method for advective
840 transport in fractures with diffusion into finite matrix blocks, *Water Resour. Res.*,
841 *37*(3), 831–835, doi:10.1029/2000WR900367.

842 van Breukelen, B. M. (2003), Natural Attenuation of Landfill Leachate:: a Combined
843 Biogeochemical Process Analysis and Microbial Ecology Approach, Ipskamp.

844 Wen, X.-H., and J. J. Gómez-Hernández (1996), The Constant Displacement Scheme
845 for Tracking Particles in Heterogeneous Aquifers, *Ground Water*, *34*(1), 135–142,
846 doi:10.1111/j.1745-6584.1996.tb01873.x.

847 Willmann, M., G. W. Lanyon, P. Marschall, and W. Kinzelbach (2013), A new
848 stochastic particle-tracking approach for fractured sedimentary formations, *Water*
849 *Resour. Res.*, *49*(1), 352–359, doi:10.1029/2012WR012191.

850 Zhang, R., S. Hu, and X. Zhang (2006), Experimental Study of Dissolution Rates of
851 Fluorite in HCl--H2O Solutions, *Aquat. Geochemistry*, *12*(2), 123–159,
852 doi:10.1007/s10498-005-3658-3.

853 Zhang, Y., and D. A. Benson (2008), Lagrangian simulation of multidimensional
854 anomalous transport at the MADE site, *Geophys. Res. Lett.*, *35*(7),
855 doi:10.1029/2008GL033222.

Tables

*Table 1: Simulation parameter values used in example 1.**

	A	B	C
$(\mu_x, \sigma_x)_{initial}$	$(40, 6)$	$(50, 6)$	–
$m_{initial}$	1 mol	1 mol	0
α, β, γ	2.3	1.3	1
θ (eq. 37)	2.3	1.3	–
R	1	1	1
k_f	$6\ (\mathrm{mol/m^3})^{-2.6}\ \mathrm{day^{-1}}$		
q	0.3 m/day		
ϕ	0.25		
D	$0.4\ \mathrm{m^2/day}$		
τ	80 days		

* $(\mu_x, \sigma_x)_{initial}$ are the mean and standard deviation defining the initial normal distribution of solute particles in space, $m_{initial}$ is the total amount of substance at the start of the simulation, and τ is the total simulated time. The other variables are defined in the text.

*Table 2: Simulation parameter values used in example 2.**

	CH_2O	O_2	CO_2
$(\mu_x, \sigma_x)_{initial}$	$(70, 2)$	$(50, 8)$	–
$m_{initial}$	1 mol	1 mol	0
α, β, γ	1	1	1
K_{CH_2O}, K_{O_2} (eq.39)	$1.6667\ \mathrm{mol/m^3}$	$0.0156\ \mathrm{mol/m^3}$	–
R	3	1	1
k_f	$0.15\ (\mathrm{mol/m^3})\ \mathrm{day^{-1}}$		

$\boldsymbol{q}$	$\mathbf{0.32\ m/day}$
$\boldsymbol{\phi}$	$\mathbf{0.25}$
$\boldsymbol{D}$	$\mathbf{0.5\ m^2/day}$
$\boldsymbol{\tau}$	$\mathbf{65\ days}$

* $(\boldsymbol{\mu_x}, \boldsymbol{\sigma_x})_{\boldsymbol{initial}}$ are the mean and standard deviation defining the initial normal distribution of solute particles in space, $\boldsymbol{m_{initial}}$ is the total amount of substance at the start of the simulation, and τ is the total simulated time. The other variables are defined in the text.

*Table 3: Simulation parameter values used in example 3.**

	$\mathbf{Ca^{2+}}$	$\mathbf{CO_3^{2-}}$	$\mathbf{CaCO_3}$
$(\boldsymbol{\mu_x}, \boldsymbol{\sigma_x})_{\boldsymbol{initial}}$	$\mathbf{(25, 5)}$	$\mathbf{(35, 8)}$	–
$\boldsymbol{m_{initial}}$	$\mathbf{2.5\ mol}$	$\mathbf{2.5\ mol}$	$\mathbf{0}$
$\boldsymbol{\alpha, \beta, \gamma}$	$\mathbf{1}$	$\mathbf{1}$	$\mathbf{1}$
$å_{Ca^{2+}}, å_{CO_3^{2-}}$ (eq. 43)	$\mathbf{0.6\ nm}$	$\mathbf{0.5\ nm}$	–
$\boldsymbol{R}$	$\mathbf{1}$	$\mathbf{1}$	∞

$\boldsymbol{k_{obs}}$	$\mathbf{0.002\ (mol/m^3)^{-2.6}\ day^{-1}}$
$\boldsymbol{k_{eq}}$	$\mathbf{10^{-2.3}\ (mol/m^3)^2}$
$\boldsymbol{q}$	$\mathbf{0.1\ m/day}$
$\boldsymbol{\phi}$	$\mathbf{0.25}$
$\boldsymbol{D}$	$\mathbf{0.15\ m^2/day}$
$\boldsymbol{\tau}$	$\mathbf{100\ days}$

* $(\boldsymbol{\mu_x}, \boldsymbol{\sigma_x})_{\boldsymbol{initial}}$ are the mean and standard deviation defining the initial normal distribution of solute particles in space, $\boldsymbol{m_{initial}}$ is the total amount of substance at the start of the simulation, and τ is the total simulated time. The other variables are defined in the text.

*Table 4: Simulation parameter values used in example 4.**

	$\mathbf{H^+}$	$\mathbf{Ca^{2+}}$	$\mathbf{HF^0}$
$(\boldsymbol{\mu_x}, \boldsymbol{\sigma_x})_{\boldsymbol{initial}}$	$\mathbf{(90, 5)}$	$\mathbf{(90, 20)}$	–
$\boldsymbol{m_{initial}}$	$\mathbf{2\ mol}$	$\mathbf{4\ mol}$	$\mathbf{0}$
$\boldsymbol{\alpha, \beta, \gamma}$	$\mathbf{2}$	$\mathbf{1}$	$\mathbf{2}$

$\boldsymbol{\theta}$ (eq. 45)	$\mathbf{1.6}$	$\mathbf{-0.8}$	–
$\boldsymbol{R}$	$\mathbf{1}$	$\mathbf{1}$	$\mathbf{1}$
$\boldsymbol{k_f}$	$\mathbf{0.72\ (mol/m^3)^{0.2}\ day^{-1}}$		
$\boldsymbol{q}$	$\mathbf{0.5\ m/day}$		
$\boldsymbol{\phi}$	$\mathbf{0.25}$		
$\boldsymbol{D}$	$\mathbf{0.4\ m^2/day}$		
$\boldsymbol{\tau}$	$\mathbf{7\ days}$		

* $(\boldsymbol{\mu_x}, \boldsymbol{\sigma_x})_{\boldsymbol{initial}}$ are the mean and standard deviation defining the initial normal distribution of solute particles in space, $\boldsymbol{m_{initial}}$ is the total amount of substance at the start of the simulation, and τ is the total simulated time. The other variables are defined in the text.

Figures

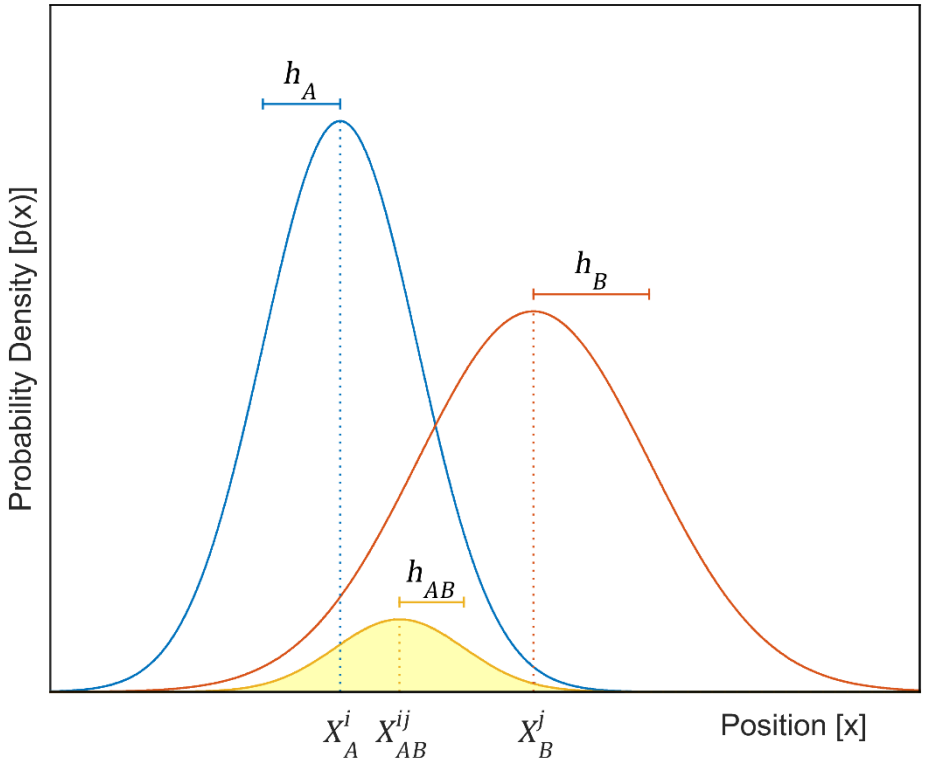

Figure 1: Schematic example of a product between two Gaussian pdf's in one dimension. The product (yellow) is another Gaussian function centered in X_{AB} and with

a standard deviation $h_{ab} = \sqrt{H_{AB}}$. Its integral over x is the probability of collocation of the two particles.

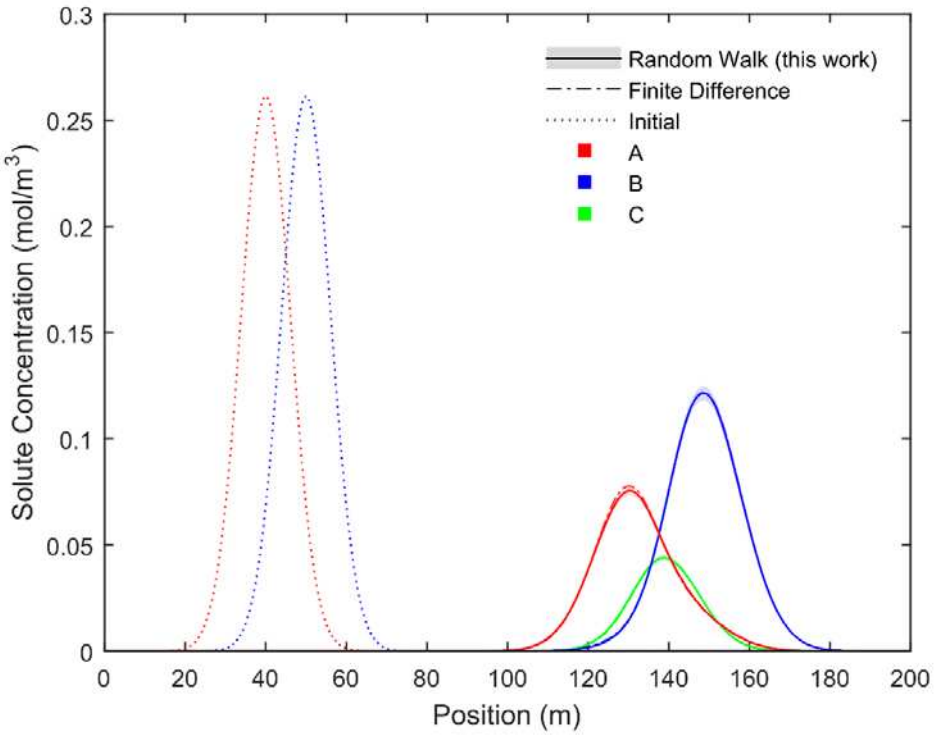

Figure 2: Solute concentrations in example 1, at the start of the simulation and after 80 days. The error zone around the Particle Tracking curves indicates ±1 standard deviation.

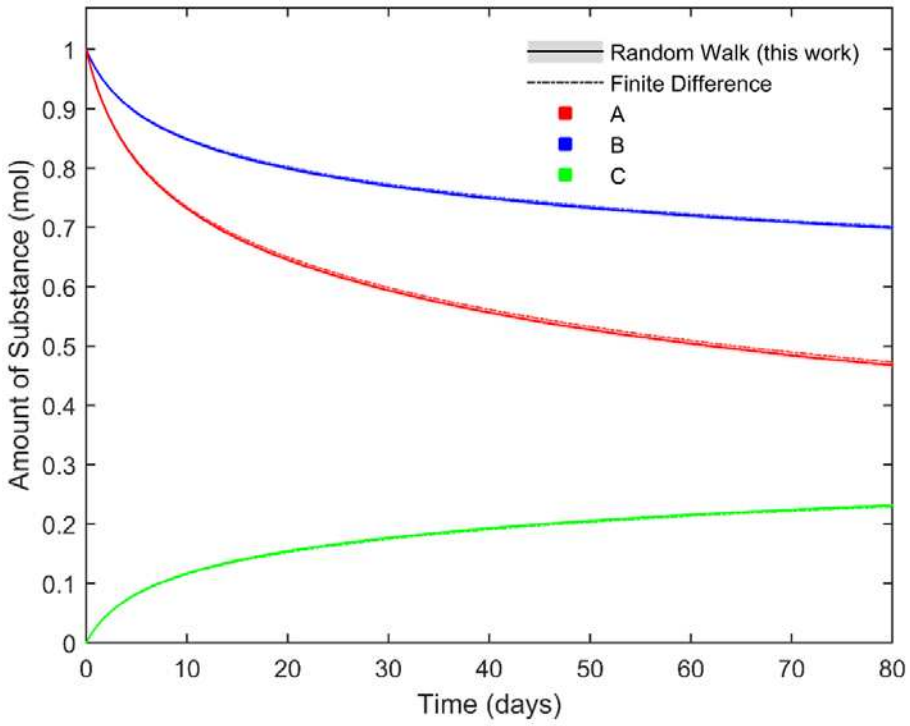

892

893 *Figure 3: Evolution in time of the total amount of substance of each compound in*
894 *example 1. The error zone around the Particle Tracking curves indicates ±1 standard*
895 *deviation.*

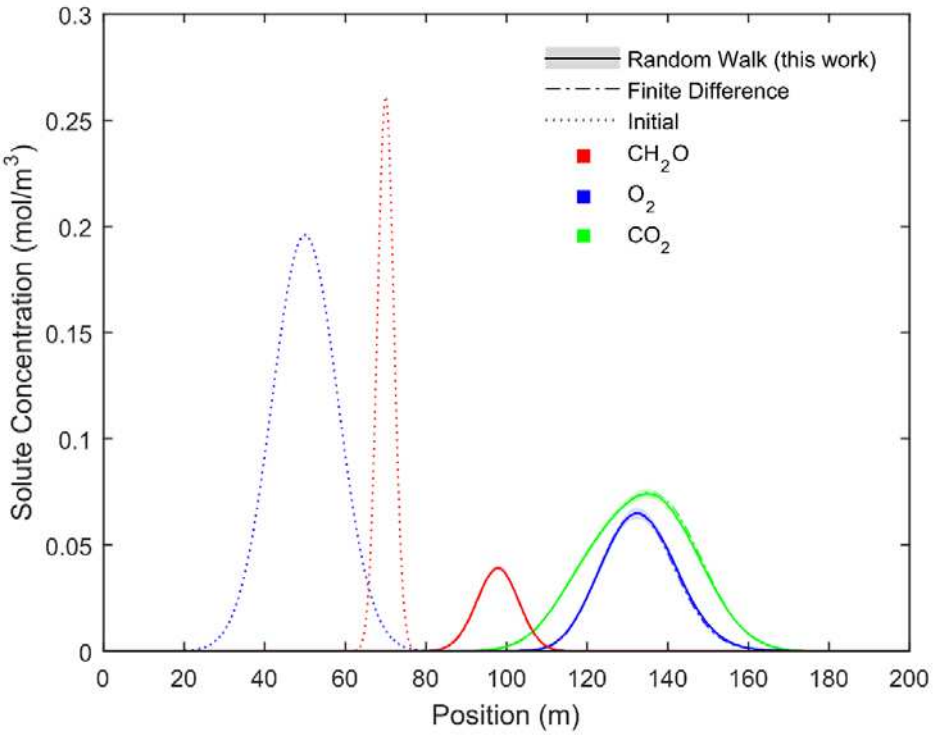

896

897 *Figure 4: Solute concentrations in example 2, at the start of the simulation and after 65*
898 *days. The error zone around the Particle Tracking curves indicates ±1 standard*
899 *deviation.*

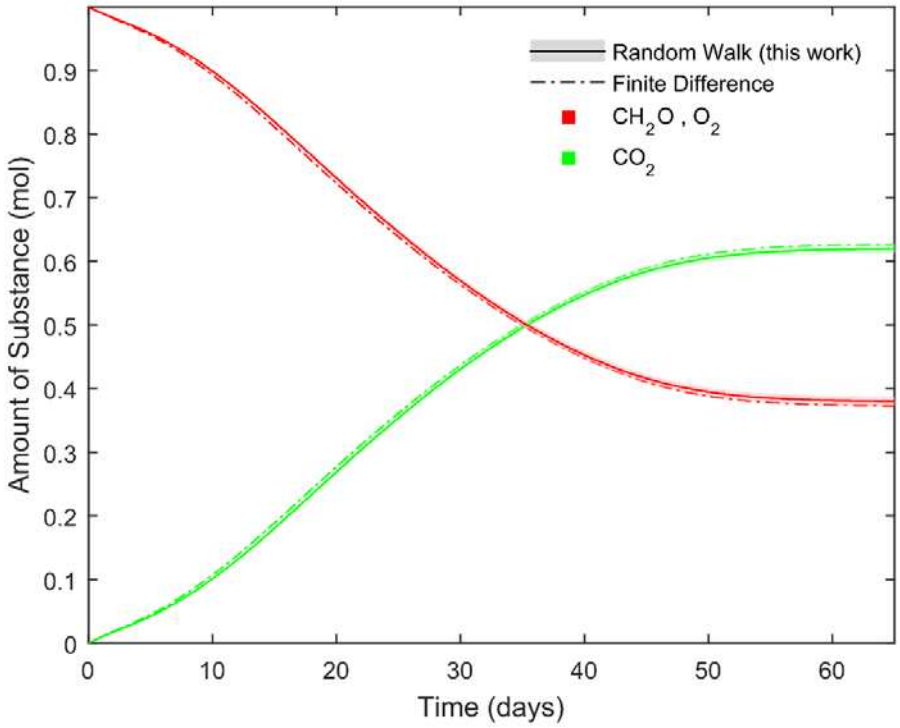

Figure 5: Evolution in time of the total amount of substance of each compound in example 2. The error zone around the Particle Tracking curves indicates ±1 standard deviation.

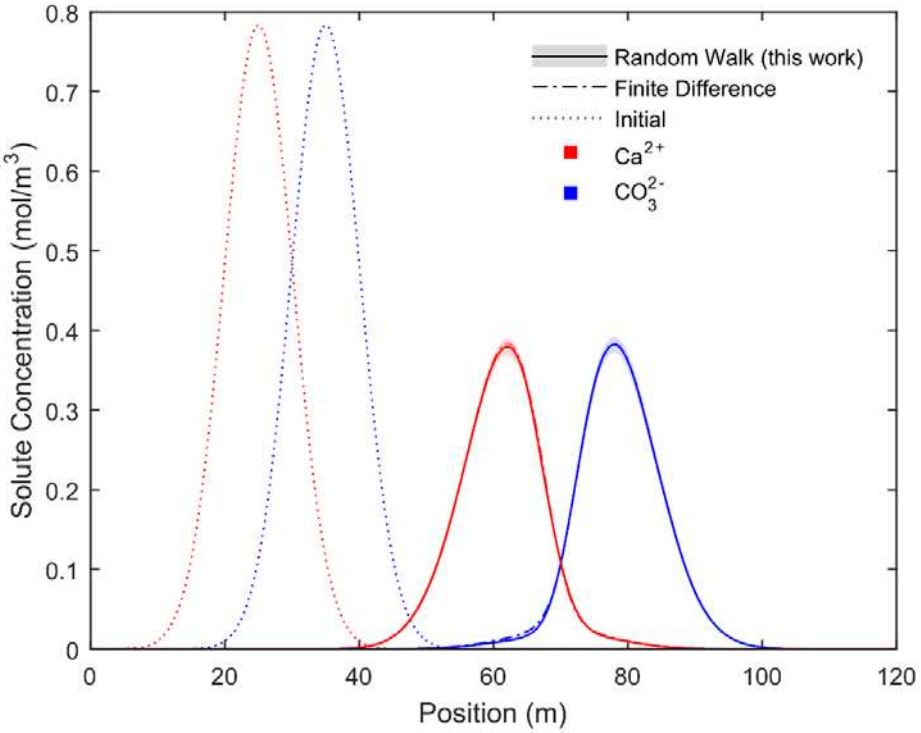

Figure 6: Solute concentrations in example 3, at the start of the simulation and after 100 days. The error zone around the Particle Tracking curves indicates ±1 standard deviation.

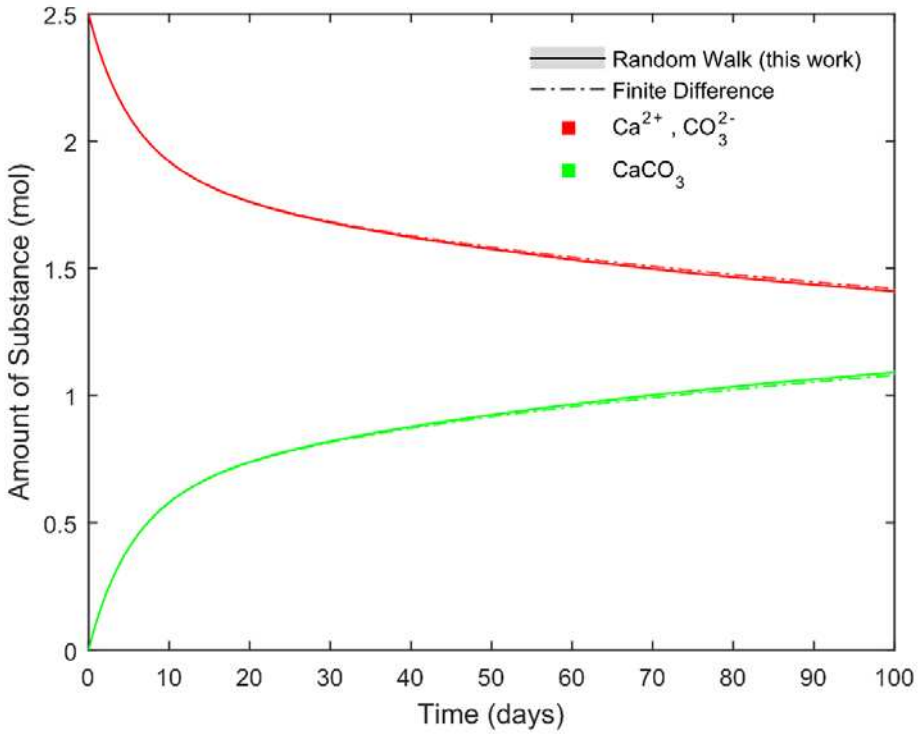

Figure 7: Evolution in time of the total amount of substance of each compound in example 3. The error zone around the Particle Tracking curves indicates ±1 standard deviation.

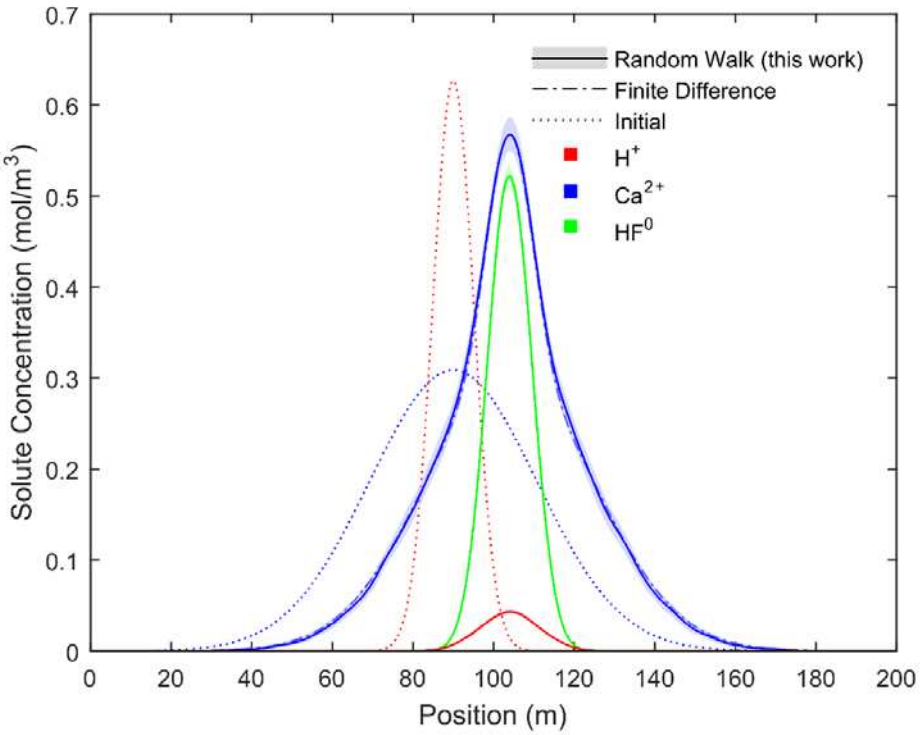

Figure 8: Solute concentrations in example 4, at the start of the simulation and after 7 days. The error zone around the Particle Tracking curves indicates ±1 standard deviation.

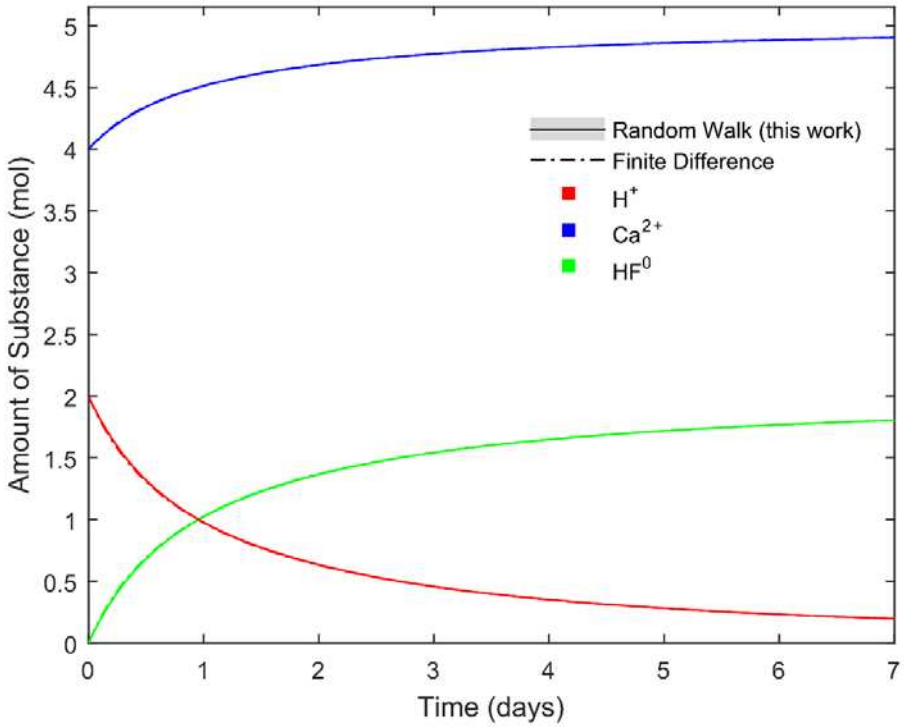

Figure 9: Evolution in time of the total amount of substance of each compound in example 4. The error zone around the Particle Tracking curves indicates ±1 standard deviation.

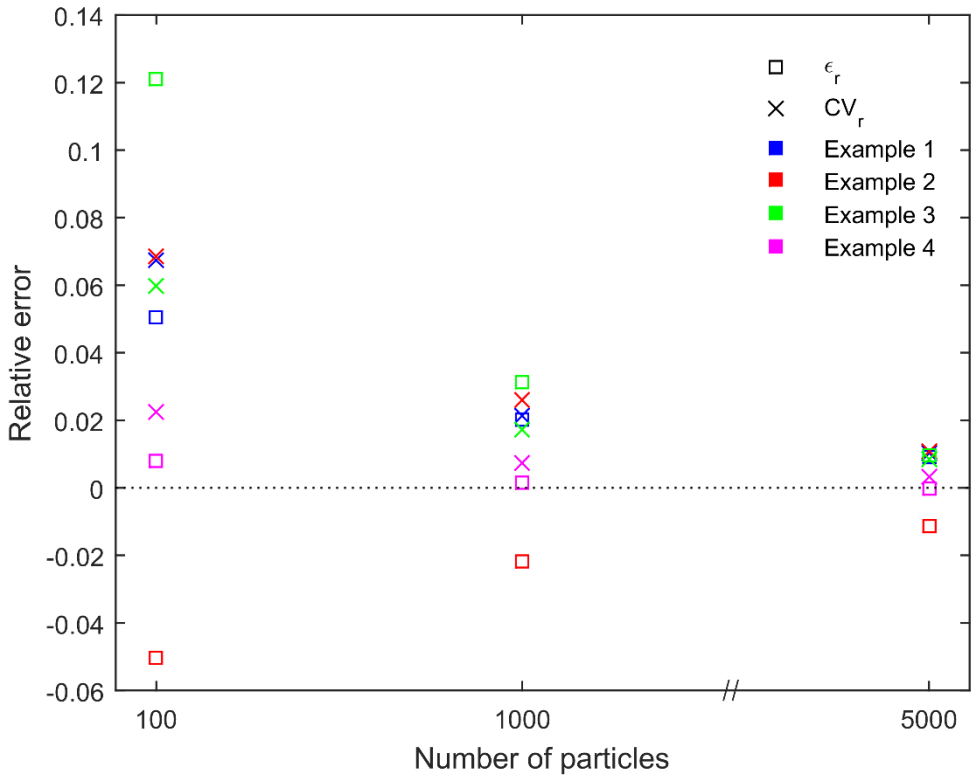

Figure 10: The two measured error components for different initial number of particles of the reactants.

923